MASTERARBEIT / MASTER'S THESIS

Titel der Masterarbeit / Title of the Master's Thesis

„The nervous system of cheilostome bryozoans"

verfasst von / submitted by

Jakob Proemer, BSc

angestrebter akademischer Grad / in partial fulfilment of the requirements for the degree of

Master of Science (MSc)

Wien, 2020 / Vienna 2020

Table of contents

Abstract

Bryozoans are sessile aquatic suspension feeders in mainly marine, but also freshwater habitats. Most species belong to the marine and calcified Cheilostomata. Since this taxon remains mostly unstudied regarding their neuroanatomy, the focus of this study is the characterization and ground pattern reconstruction of the autozooidal nervous system of this taxon. Two classical and two modern neuronal tracing techniques were tested and evaluated for future neuroanatomical studies. The analysis is based on data from six representatives of several major cheilostome taxa. Results reveal a common innervation pattern in the investigated species. The cerebral ganglion is located at the base of the lophophore, from where neurite bundles embrace the mouth opening to form a circumoral nerve ring. Four neurite bundles project from the cerebral ganglion to innervate peripheral areas, such as the body wall and parietal muscles via the tentacle sheath. Five neurite bundles comprise the main innervation of the visceral tract. Four neurite bundles innervate each tentacle via the circumoral nerve ring. Mediofrontal tentacle neurite bundles emerge directly from the nerve ring. Two laterofrontal- and one abfrontal tentacle neurite bundles emanate from radial neurite bundles, which originate from the cerebral ganglion and circumoral nerve ring in between two adjacent tentacles. The radial neurite bundles terminate in intertentacular sites and give rise to one abfrontal neurite bundle at the oral side and two abfrontal neurite bundles at the anal side. Similar patterns are described in ctenostome bryozoans. The present result thus represents the gymnolaemate situation. Innervation of the tentacle sheath and visceral tract by fewer neurite bundles and tentacular innervation by four to six tentacle neurite bundles support cyclostomes as sister taxon to gymnolaemates. Phylactolaemates feature fewest distinct neurite bundles in visceral- and tentacle sheath innervation, which always split in nervous plexi and their tentacles have six neurite bundles. Thus, this study supports phylactolaemates as sistergroup to myolaemates.

1. Introduction

1.1 General information and morphology of bryozoans

Bryozoans are small, colonial and mainly sessile filter feeders. About 6,000 species are extant in this lophotrochozoan taxon, which consists of three major subordinate taxa (Mukai et al., 1997). With about 100 species, the entirely limnetic Phylactolaemata are the smallest taxon (Massard & Geimer, 2008; Waeschenbach et al., 2012). Stenolaemata and Gymnolaemata form the taxon Myolaemata that possess an apomorphic myoepithelial and triradiate pharynx (Schwaha et al., 2019, 2020). The marine taxon Stenolaemata is represented by only one extant taxon with about 700 species, the Cyclostomata (Waeschenbach et al., 2012). Gymnolaemata separate in two clades: the rather small and paraphyletic group of "Ctenostomata" live in marine, brackish and freshwater habitats and comprise about 300 species (Waeschenbach et al., 2012); more than 5,000 species belong to the taxon Cheilostomata, the largest group of Bryozoa (Waeschenbach et al., 2012; Martha et al., 2016). Cheilostomes are mainly marine, with some brackish representatives (Waeschenbach et al., 2012).

Bryozoan colonies vary in size between centimeters and one meter (Ryland, 2005). They are formed by sexually reproduced, planktonic larvae. Once settled on suitable substrate, larvae undergo metamorphosis to the founding zooid (the single module) of a bryozoan colony called ancestrula (Fig. 1A, 1C). During colonial growth (astogeny) more zooids are formed by asexual budding in distal direction with respect to the mother zooids position (Ryland, 1977; Schwaha, in press). Colonies follow seasonal growth patterns with full regressions at the end of each season (Hayward & Ryland, 1975).

Every single zooid consists of a body wall called cystid, and an internal, movable soft body, called polypide (Mukai et al., 1997). Two of the three orientation axes, the proximo-distal-axis and the fronto-basal axis relate to the cystid of a zooid. The oral-anal axis is only applicable to the polypide. The cystid is calcified in cyclostomes and cheilostomes (Ryland, 2005). It has an internal cellular layer, the endocyst, that secretes an outer layer, the ectocyst (Mukai et al., 1997). Bryozoans retract the polypide into the cystid via a prominent retractor muscle. Due to the differences in cystid architecture, the three major taxa use different mechanisms for polypide protrusion: (1) Phylactolaemates use orthogonal body wall musculature to increase coelomic pressure (Gawin et al., 2017; Schwaha et al., 2020; Schwaha, in press). (2)

2

Cyclostomes increase coelomic pressure with a membranous sac derived from their peritoneum that bears annular muscles (Nielsen & Pedersen, 1979; Schwaha et al., 2020; Schwaha, in press). (3) Gymnolaemates use parietal musculature to increase pressure in their body cavity (Schwaha et al., 2020; Schwaha, in press).

The polypide is composed of a tentacle crown called lophophore, a u-shaped digestive tract, musculature and the nervous system (Fig. 2). The lophophore of Phylactolaemata is horseshoe-shaped, whereas the lophophore of myolaemates is circular (Ryland, 2005). It bears tentacles used for upstream feeding. The main orientation axis concerning the tentacles is frontal-abfrontal. In an everted polypide, the frontal side of a tentacle faces the feeding current. The tentacles are ciliated with frontal cilia that move food particles towards the mouth in all taxa except for cyclostomes that use a mucous instead (Riisgård et al., 2010; Schwaha et al., 2018). Lateral cilia create a water current towards the abfrontal side of the tentacles. Laterofrontal cilia act as a filter to retain food particles (Nielsen & Riisgård, 1998). The abfrontal cilia are part of so-called abfrontal sensory organs (Nielsen & Riisgård, 1998). The main food sources are most likely bacteria and phytoplankton (Ryland, 1977). The digestive tract is differentiated into a foregut (pharynx and esophagus), a midgut (cardia, blind ending caecum and pylorus), a hindgut (intestine) and an anus (Mukai et al., 1997). While the whole digestive tract of phylactolaemates bears prominent musculature, the pharynx is the main muscular structure in the digestive tract of myolaemates (Schwaha et al., 2019). The anus is situated outside of the lophophore, eponymous for the bryozoans' morphological designation, ectoprocts. The nervous system of bryozoans is centered at the lophophoral base, from where it innervates the remaining parts of the polypide.

1.2 Gymnolaemate nervous system architecture

Cerebral ganglion

All bryozoans possess a cerebral ganglion at the anal side at the base of the lophophore (Gruhl & Bartolomaeus, 2008; Weber et al., 2014; Schwaha & Wanninger, 2015; Temereva & Kosevich, 2016; Schwaha et al., 2020; Schwaha, in press). It most likely had a central lumen in the last common ancestor (Gruhl & Schwaha, 2015; Schwaha et al., 2020; Schwaha, in press). Concerning Gymnolaemata, few detailed information is available. From the cerebral ganglion, a circumoral nerve ring and nine neurite bundles emanate to innervate the three main parts of the polypide.

Neurite bundles of the tentacle sheath

The circumoral nerve ring surrounds the mouth opening from the lateral sides of the cerebral ganglion (Schwaha et al., 2020). Four of the nine main neurite bundles emanate directly from the cerebral ganglion in distal direction to innervate aperture associated- and parietal muscles via the tentacle sheath (Weber et al., 2014; Schwaha & Wanninger, 2015; Temereva & Kosevich, 2016; Schwaha et al., 2020; Schwaha, in press). A pair of direct tentacle sheath neurite bundles emanate from the cerebral ganglion (Lutaud, 1977a; Weber et al., 2014; Schwaha & Wanninger, 2015; Temereva & Kosevich, 2016). A pair of trifid neurite bundles joins them (Weber et al., 2014; Temereva & Kosevich, 2016). The trifid neurite bundles emanate from the cerebral ganglion in lateral direction to bend perpendicularly in distal direction (Weber et al., 2014; Temereva & Kosevich, 2016). They fuse with the direct tentacle sheath neurite bundles close to the lophophoral base to form a compound tentacle sheath neurite bundle (Lutaud, 1977a; Weber et al., 2014; Schwaha & Wanninger, 2015; Temereva & Kosevich, 2016).

Visceral innervation

Proximally of the lophophore lies the visceral tract (Fig. 2). Its innervation is mostly restricted to the pharynx, along of which the remaining five neurite bundles of the cerebral ganglion extend in proximo-distal direction and terminate at the cardia, at the proximal end of the pharynx (Lutaud, 1977a; Weber et al., 2014; Temereva & Kosevich, 2016; Schwaha et al., 2020; Schwaha, in press). One mediovisceral, two laterovisceral and two lateromediovisceral neurite bundles embrace the pharynx and give rise to a circumpharyngeal nerve plexus that fully surrounds the pharynx. (Lutaud, 1977a; Gruhl & Schwaha, 2015).

Peripheral innervation

The trifid neurite bundles have three branches each (Lutaud, 1973a, 1977a; Temereva & Kosevich, 2016). The main branch joins the direct tentacle sheath neurite bundles after a perpendicular bend at the lateral sides of the cerebral ganglion. One small branch projects towards the pharynx from the most lateral part of each main branch (Lutaud, 1973b). A third branch embraces parts of the tentacle sheath as annular branch (Lutaud, 1973b, 1977a). The compound tentacle sheath neurite bundles project towards the orifice, the terminal opening of a zooid, via duplicature bands (Lutaud, 1973b; Schwaha et al., 2020). The latter are muscle bands of still unknown function.
4

The compound tentacle sheath neurite bundles split into four neurite bundles at their distal end to innervate apertural- and parietal muscles (Lutaud, 1973a). The term aperture associated muscles refers to diaphragmatic sphincter muscles, parietodiaphragmatic muscles and the ctenostome parietovestibular/cheilostome operculum occlusor muscles (Schwaha, in press).

The polypide retractor is the most prominent muscle in a zooid and connects the lophophore with the cystid (Schwaha, in press). It is innervated via small neurite bundles that extend along each muscle fiber and originate from the trifid neurite bundles (Bronstein, 1937; Lutaud, 1977a). The number of neurite bundles innervating the three parts of the polypides is taxon specific for major bryozoan clades (Schwaha, in press).

Tentacular innervation

The cerebral ganglion and the circumoral nerve ring form the basis of the lophophore and tentacle innervation. Four to six tentacle neurite bundles emanate directly from the cerebral ganglion and the circumoral nerve ring into each tentacle (Lutaud, 1977a; Weber et al., 2014; Gruhl & Schwaha, 2015; Temereva & Kosevich, 2016; Schwaha et al., 2020; Schwaha, in press). At the lophophoral base, in between the tentacles are so called intertentacular pits bearing perikarya (Schwaha & Wanninger, 2015; Schwaha, in press). In cheilostomes, tentacles are innervated by four neurite bundles each, one along the mediofrontal side, one along the abfrontal side and two along the laterofrontal sides of each tentacle (Lutaud, 1977a; Weber et al., 2014; Temereva & Kosevich, 2016; Schwaha, in press).

1.3 Early approaches in bryozoan neuroanatomical research

Early research on the bryozoan nervous system focused on large species with transparent cystids that were easily accessible. This is mainly the case in phylactolaemate bryozoans. This small taxon has been comparatively well investigated over the past century and the past decade (Gerwerzhagen, 1913; Shunkina et al., 2015; Ambros et al., 2018). Most past research was based on methylene blue vital staining (Gerwerzhagen, 1913; Marcus, 1926; Graupner, 1930; Bronstein, 1937). Very few authors investigated marine as well as freshwater bryozoans (Marcus, 1926; Graupner, 1930). Concerning cheilostomes, first comprehensive analyses focused on the nervous system of *Electra pilosa* (Lutaud, 1969, 1973b, 1973a, 1979a, 1980, 1982a). The studies were conducted much later but still used methylene blue vital- and

silver staining. Apart from *E. pilosa* only *Membranipora membranacea* was studied with respect to its full autozooidal neuroanatomy. The species *Bugula calathus*, *Cartella papyracea* and *Cryptosula pallasiana* were only partly studied (Bronstein, 1937; Gordon, 1974; Lutaud, 1982b).

In recent years cyclostome and ctenostome species were analyzed with state-of-the-art techniques, providing valuable insights in comparative bryozoan neuroanatomy (Weber et al., 2014; Temereva & Kosevich, 2016; Schwaha et al., 2018; Temereva & Kosevich, 2018; Worsaae et al., 2018; Pröts et al., 2019). Immunolabelling (immunocytochemistry, ICC) techniques in combination with confocal laser scanning microscopy (CLSM) are state-of-the-art methods used in morphology. With its invention, the methodologic border to conduct a study including several species was overcome. These combined methods allow time efficient experiments that promise clear and easily reproducible data. After a comprehensive study on the serotonergic nervous system in Gymnolaemata (Schwaha & Wanninger, 2015) and few studies of ctenostome species (Weber et al., 2014; Temereva & Kosevich, 2016; Pröts et al., 2019), this study is the first to use this approach to investigate the autozooidal nervous system focusing on Cheilostomata.

1.4 Study goals

Since cheilostomes are the most diverse bryozoan taxon and remain mostly unstudied regarding their neuroanatomy, this study aims to create a representative set of neuroanatomical data, based on six species out of four major taxa (Fig. 3A, 4A, 5A, 6A, 7A, 8A). A character matrix based on previous research forms the basis of a comparative analysis. The collected data is used to construct a hypothetical ground pattern of the nervous system of cheilostome bryozoans. Additionally, four methods were tested and evaluated against each other in an integrative approach.

2. Material and Methods

2.1 Sampling, identification and fixation

Six species from four major cheilostome taxa were used in the experiments (Tab. 1). They were sampled from different substrate types at Valsaline Bay, Pula, in Istria, Croatia (44°51'59'' N, 13°50'01'' E) in May and June 2019. The four species *Electra posidoniae* (Fig. 3A), *Fenestrulina joannae* (Fig. 4A), *Collarina balzaci* (Fig. 7A) and *Chorizopora brongniartii* (Fig. 8A) were found on the seagrass *Posidonia oceanica*.

Myriapora truncata (Fig. 5A) was found growing on secondary hard bottoms and *Bugula neritina* (Fig. 6A) was found growing on hard substrate. Samples were identified using a bryozoan identification guide by Zabala and Maluquer (1988) under a Nikon SMZ25 stereomicroscope (Nikon, Chiyoda, Tokyo, Japan). Identification was documented with a Nikon DS-Ri2 microscope camera (Nikon, Chiyoda, Tokyo, Japan). The species were assigned to one of three colony morphologies according to Hageman et al. (1998): (1) encrusting with fused structural units (Fig. 1A), (2) erect branching with biserial arrangement of zooids (Fig. 1B), and (3) erect with solid branches and radial arrangement of zooids (Fig. 1D).

Four different methods were applied to the samples (Tab. 1). The well-established ICC labelling against acetylated α-tubulin was used to collect data on general nervous system architecture. Comparative experiments were conducted with methylene blue vital staining, silver staining of the nervous system and neuronal tracing with the fluorescent tracer 1,1′-Dioctadecyl-3,3,3′,3′-tetramethylindocarbocyanine perchlorate (DiI). Samples treated with ICC, DiI and the Bubernaite modification of silver staining were fixed in 4 % paraformaldehyde (PFA) in 0.1 M phosphate buffered saline with pH of 7,4 (PBS) for 1 h. After washing them three times for 1 h each in PBS they were stored in PBS with 0.01 % sodium azide. Fixation of animals for the remaining protocols are stated at the respective sections.

2.2 Sample preparation

2.2.1 Immunocytochemistry

If not stated otherwise, all incubation steps were performed at room temperature. Samples were incubated in 20 % ethylenediaminetetraacetic acid (EDTA) in water for 1 h or 24 h depending on their calcification state prior to application of the respective staining techniques (Tab. 1).

Decalcified samples of all six species were washed two times 20 min each in PBS and incubated in a blocking solution of 6 % normal goat serum (Thermo Fisher Scientific, Waltham, MA, USA), 2 % dimethyl sulfoxide (DMSO) and 2 % Triton X-100 in PBS overnight. They were incubated with a monoclonal antibody against acetylated α-tubulin raised in mouse (T6793, Sigma Aldrich, St. Louis, MO, US) diluted 1:600 in PBS with 2 % DMSO and 2 % Triton X-100 over night. After being washed with PBS four times 20 min each, they were incubated in goat anti mouse Alexa Fluor 568 (A11004, Thermo Fisher Scientific, Waltham, MA, USA) in 1:300 dilution together with

DAPI (D1306, Thermo Fisher Scientific, Waltham, MA, USA) in 1:100 dilution and Alexa Fluor 488 Phalloidin (A12379, Thermo Fisher Scientific, Waltham, MA, USA) in 1:40 dilution with 2 % DMSO and 2 % Triton X-100 in PBS overnight. Samples were washed four times 20 min each with PBS and mounted in Fluoromount G (Southern Biotech, Birmingham, AL, USA). They were kept at 4 °C overnight for hardening of the mounting medium and subsequently analyzed using a Leica SP5 II CLSM (Leica Microsystems, Wetzlar, Germany). Scans were acquired with optical slices of 0.6 μm to 0.13 μm, depending on magnification used and the quality of the immunolabelling.

2.2.2 Methylene blue vital staining

Three experiments were made with methylene blue. Protocols for the experiments were adapted after Gerwerzhagen (1913), Bronstein (1937) and Lutaud (1969). This experiment was conducted as soon as possible after sampling, at latest five days. In a first experiment, the dye was diluted in freshwater of which drops were added to the sample. The sample was checked every 10 min to see if the dye would work. When no staining was visible after 1 h 30 min the experiment was stopped. In a second experiment, the dye was added to sea water in the exact same dilution and way but the samples were fixed in 5 % ammonium molybdate together with drops of osmium tetroxide for 20 h after 1 h of incubation with methylene blue. In a third experiment, the dye was added directly into sea water and the sample was incubated for 1 h and 30 min. Samples were again fixed in a solution of 5 % ammonium molybdate with drops of osmium tetroxide for 20 h. All samples were mounted in glycerol and observed under a Nikon NiU with a DsRi2 microscope camera (Nikon, Tokyo, Japan).

2.2.3 Silver staining of the nervous system

Three experiments were conducted using silver staining of the nervous system. The protocols were modified from the standard protocols after Bubernaite, Golgi-Collonier-Golgi and Kallius, which are well established for histological sections of vertebrates (Aescht et al., 2015). They were adapted for use in small wholemounts.

In the Bubernaite modification of the protocol, PFA fixed material was incubated in 1.25 % potassium dichromate solution (PDC) for either two, three or four days. They were briefly washed in 0.75 % silver nitrate (SN) before being incubated in SN for four, three or two days in the dark. The SN incubation time complemented PDC incubation time so that the full incubation time for each sub experiment came to be six days. Samples

were washed and dehydrated in an ascending ethanol series for 5 min each. The 100 % step was repeated three times before samples were stored in 0.5 ml glycerol.

Animals used in the Golgi-Collonier-Golgi rapid method were fixed in fresh Golgi fixative composed of 1 % PFA, 0.002 % calcium chloride and 1 % glutaraldehyde in 0.1 M PBS. They were directly used for the experiment. Fixed material was decalcified in 20 % EDTA and washed in 2.5 % PDC three times for 30 min each. They were incubated in 2.5 % PDC with drops of 1 % osmium tetroxide for three days. Samples were washed in SN until no more precipitate would come off the sample. They were incubated in SN three more days. Samples were washed directly with 70 % ethanol and put in an ascending ethanol series before being stored in 0.5 ml glycerol for examination. A small portion of the sample was decalcified in 20 % EDTA only after SN incubation as additional experiment.

Animals used in the Kallius modification of silver staining were fixed in Golgi fixative composed of 40 ml 2.5 % PDC and 10 ml of 1 % osmium tetroxide overnight at 4 °C and directly used for the experiment. Half of this sample was fixed at room temperature as additional experiment. All of the sample was washed in SN until no more PDC reacted with the SN in the embryo dish. Samples were washed in 80 % ethanol three times. They were kept in 0.5 % hydroquinone for 5 min and washed in 70 % ethanol. All samples were washed in 20 % sodium sulfite before being washed three times 5 min each in 20 % EDTA and being stored in 20 % EDTA overnight for decalcification. They were put in an ascending ethanol series and stored in 0.5 ml glycerol.

All silver stained specimens were analyzed under a Nikon NiU with a DsRi2 microscope camera (Nikon, Tokyo, Japan). Parts of each samples were dissected before being mounted.

2.2.4 Neuronal tracing with DiI

Neuronal tracing was performed with the encrusting bryozoan species *E. posidoniae* in a protocol modified after Stemme et al. (2014). A plane petri dish was coated in DiI (Sigma Aldrich, St. Louis, MO, US) by pouring the methanol dissolved tracer into the petri dish and leaving the dish in a foam hood until the methanol was fully evaporated. Colony pieces of 5-10 zooids in size were placed on the DiI layer with forceps, so that the basal side of the colony faced the tracer. The colony pieces were covered with hardened pieces of 1.5 % LE agarose (Biozym Scientific GmbH, Hessisch Oldendorf, Germany). Agarose pieces maintained physical contact between animals and crust

after closing the petri dish. Samples were incubated at 4 °C for two weeks in the dark. They were mounted in Fluoromount G and stored at 4 °C for one night, before being scanned with a Leica SP5 II CLSM (Leica Microsystems, Wetzlar, Germany). DiI scans were recorded with optical slice thickness of 0.4 µm.

2.3 Data Analysis

ICC was the only method applied to all specimens. Only ICC data were used for the characterization of the nervous system. The remaining methods were evaluated against each other. All zooids were examined in a retracted position. Characters for evaluation of the nervous system were defined using terminologies of Richter et al. (2010), Lutaud (1977a), Mukai et al. (1997), Gruhl and Schwaha (2015) and Schwaha (in press). The center of the nervous system is referred to as cerebral ganglion, based on most recent terminology (Schwaha, in press). All image stacks were analyzed using Amira, version 6.4 (FEI, Hillsboro, Oregon, USA). Morphological characters were evaluated as nervous system character matrix (Tab. 2). Deviations from the ground pattern in the studied species are most likely due to preparation errors. A ground pattern analysis was performed based on the matrix and data from previous studies (Tab. 3). "Ctenostomata" are the outgroup in this study. Three character states were defined for the analysis: absent (1), present (0), inapplicable (-).

3. Results

3.1 Overviews on morphology and myoanatomy

In *Electra posidoniae*, the operculum is autofluorescent (Fig. 3B). Prominent operculum occlusor muscles attach to the operculum (Fig. 3B). Below the operculum is the vestibulum, a cavity surrounded by the vestibular wall. The vestibular wall is proximally bordered by the diaphragm, marked by the diaphragmatic sphincter muscle (Fig. 3B). Proximal of the diaphragm is the tentacle sheath, from where duplicature bands project towards the cystid wall (Fig. 3B). The tentacle sheath terminates at the lophophoral base, where a prominent retractor muscle attaches (Fig. 3B). Tentacle muscles are present as two longitudinal muscle bands (Fig. 3B). The pharynx has strong ring muscles (Fig. 3B). A second, weaker muscle plexus surrounds the remaining visceral tract (Fig. 3B). Two caecum ligaments project from the midgut to the body wall, visible only in *E. posidoniae* (Fig. 3B). There are two lateral sets of parietal muscles in the body cavity of the animals (Fig. 3B). Apart from the caecum ligaments, the morphology of *E. posidoniae* is congruent with the morphologies of

10

Fenestrulina joannae (Fig. 4B) and *Myriapora truncata* (Fig. 5B). The operculum occlusor muscle is absent in *Bugula neritina* (Fig. 6B). The muscular plexus of the digestive tract is absent in *Collarina balzaci* (Fig. 7B). *Chorizopora brongniartii* has a prominent muscular plexus around the digestive tract (Fig. 8B).

3.2 Neuronal pattern of investigated species

Cerebral ganglion and directly emanating neurite bundles

The cerebral ganglion is situated at the basal side at the lophophoral base (Figs. 3D, 4D, 5D, 6D, 7D, 8D, 9A). From the cerebral ganglion, neurite bundles embrace the mouth opening as circumoral nerve ring (Figs. 3D, 4D, 5D, 6E, 7D, 9A, 9B). Two thick direct tentacle sheath neurite bundles emanate from the cerebral ganglion in distal direction on the basal side of the cerebral ganglion (Figs. 3D, 4D, 5D, 6E, 7D, 8D, 9A). A pair of trifid neurite bundles emanate from the lateral sides of the cerebral ganglion and project towards lateral (Figs. 3D, 4D, 5D, 6E, 7D, 8D, 9A). They project towards the vestibulum after a perpendicular bend (Figs. 3D, 4D, 5D, 7D, 8D). They fuse with the direct tentacle sheath neurite bundles to form compound tentacle sheath neurite bundles close to the lophophoral base (Figs. 3D, 5D, 7D, 9A). The trifid neurite bundles possess two additional branches. The first, descending branch originates at the bending of the trifid neurite bundles (Figs. 3D, 5D, 9A). The second branch separates from the trifid neurite bundles shortly before their fusion with the direct tentacle sheath neurite bundles (Figs. 3D, 5D, 6E, 9A). This so-called annular branch forms an open circle around the base of the lophophore (Figs. 3D, 5D, 6E, 9A). It is absent in *Fenestrulina joannae*, *Collarina balzaci* and *Chorizopora brongniartii* (Tab. 2). Descending branches of the trifid neurite bundles are absent in *F. joannae* (Tab. 2).

Visceral innervation

In proximal direction, the cerebral ganglion gives rise to a mediovisceral neurite bundle that extends along the basal part of the pharynx (Figs. 3D, 4D, 5D, 6D, 7D, 8D, 9A). Additionally, two laterovisceral- and two mediolaterovisceral neurite bundles innervate the muscular pharynx from the cerebral ganglion (Figs. 11A, 12A, 13A, 14A, 15A, 16A). Mediolaterovisceral neurite bundles are absent in *Fenestrulina joannae*, *Collarina balzaci* and *Chorizopora brongniartii*. All visceral neurite bundles terminate at the proximal end of the pharynx (Figs. 5D, 7D, 8C, 11A, 12A, 14A). A pharyngeal nerve plexus surrounds the pharynx and connects the visceral neurite bundles to each other

(Figs. 3D, 12A, 13A, 14A, 14A). The pharyngeal nerve plexus is absent in *C. brongniartii* (Tab. 2).

Peripheral innervation

The compound tentacle sheath neurite bundles project along basal duplicature bands and terminate at one parietal branching point each, which is located close to the diaphragm (Figs. 3E, 4E, 5E, 6C, 7E, 8E, 9A). Here, they split up into an operculum occlusor neurite bundle, a parietodiaphragmatic neurite bundle, a sphincter neurite bundle, and a parietal muscle neurite bundle (Figs. 3E, 4E, 5E, 6C, 7E, 8E, 9A). The parietal muscles are innervated by one main parietal muscle neurite bundle from which smaller neurite bundles project to the respective muscles (Figs. 3E, 6C, 8E, 9A). The parietal muscle neurite bundles and parietodiaphragmatic neurite bundles are absent in *Myriapora truncata* (Tab. 2). The opercular neurite bundle is absent in *Bugula neritina* (Tab. 2). α-tubulin is present in interzooidal pores of *Electra posidoniae* (Fig. 3C) but is absent in the interzooidal pores of all remaining examined species (Tab. 2).

Tentacular innervation

The cerebral ganglion and the circumoral nerve ring give rise to the innervation of the lophophoral base. Tentacle neurite bundles emerge directly from the cerebral ganglion on the anal side and from the nerve ring in the remaining parts of the lophophore (Figs. 9B, 17). Four neurite bundles innervate each tentacle (Figs. 9B, 11B,C, 12B,C, 13B,C, 14B,C, 15B,C, 16B,C). Mediofrontal tentacle neurite bundles emanate from the circumoral nerve ring directly into the center of each tentacle (Figs. 9B, 11B,C, 12B,C, 13B,C, 14B,C, 15B,C, 16B,C). Short radial neurite bundles also project directly from the cerebral ganglion or nerve ring to intertentacular areas where they terminate in intertentacular sites (Figs. 9B, 11B,C, 12B,C, 13B,C, 14B,C, 15B,C, 16B,C). The radial neurite bundles give rise to smaller intertentacular neurites that protrude in respective intertentacular pits (Figs. 9B, 11B,C, 12B,C, 13B,C, 14B,C, 15B,C, 16B,C). From the radial neurite bundles, abfrontal tentacle neurite bundles emanate into the tentacles to form the most prominent neurite bundles of each tentacle (Figs. 9B, 11B,C, 12B,C, 13B,C, 14B,C, 15B,C, 16B,C). Radial neurite bundles close to the cerebral ganglion form the base of two abfrontal neurite bundles of adjacent tentacles (Figs. 9B, 11B,C, 13B,C). Radial neurite bundles along the circumoral nerve ring only give rise to one abfrontal neurite bundles (Figs. 9B, 12B,C, 14B,C, 15B,C, 16B,C). All radial neurite

bundles are the basis of two laterofrontal neurite bundles that project in adjacent tentacles close to tentacle cilia (Figs. 9B, 11B,C, 12B,C, 13B,C, 14B,C, 15B,C, 16B,C).

3.3 Assessment of additional methods

Methylene blue vital staining did not deliver reliable results. No silver stained sample showed the expected signal of the innervation of a polypide. Samples of the Bubernaite experiment were only little impregnated, showing very few diffuse signal in the samples. Samples of the Golgi-Colonier-Golgi experiment show large amounts of precipitate on the cystid, but no signal at the inside in the polypides. Samples used for the Kallius-experiment show heavy precipitate on the cystid walls at both incubation temperatures. The precipitate is not translucent. The neuronal tracer DiI labelled the polypide tissue halfway through from basal to frontal, providing clear signal in one experiment (Fig. 18). The lophophore, visceral tract (pharynx, caecum, intestine) and peripheral structures (opercular muscles, parietodiaphragmatic muscles, diaphragmatic sphincter muscle, duplicature bands) were labelled (Fig. 18). Neuronal structures were labelled as well as muscles (Fig. 18).

4. Discussion

4.1 Cerebral ganglion and lophophoral base

The cerebral ganglion is situated on the anal side of the polypide at the base of the lophophore in all species (Figs. 3D, 4D, 5D, 6D, 7D, 8D). It varies in size from about 15 µm in *Chorizopora brongniartii* to about 30 µm in *Myriapora truncata* (Fig. 13A, 16A), which is similar as reported for other marine calcified bryozoans (Lutaud, 1977a; Schwaha & Wanninger, 2015; Temereva & Kosevich, 2016; Schwaha et al., 2018; Worsaae et al., 2018). This study supports a compartmentation of the cerebral ganglion in gymnolaemates as it was found in studies on the cheilostome *Electra pilosa* (Lutaud, 1969) and the ctenostome *Amathia gracilis* (Temereva & Kosevich, 2016) by similar locations of the main neurite bundles emanating from the cerebral ganglion (Figs. 3D, 4D, 5D, 7D, 14A, 16A). The main neurite bundles clearly originate from clusters of somata in different parts of the cerebral ganglion. These areas are no distinct ganglia since they lack a cortex of somata and a neuropil in the center (Richter et al., 2010). Accordingly, no compartmentation at the level of ganglia was described in two recent studies of the ctenostomes *Paludicella articulata* and *Hypophorella expansa* (Weber et al., 2014; Pröts et al., 2019). A distinction of regions in the cerebral

ganglion can only be made on the level of clusters of cell somata that give rise to the main polypide innervating neurite bundles rather than speaking of ganglia.

The cerebral ganglion of adult *Paludicella articulata* has a small fluid filled lumen (Weber et al., 2014). A similar lumen is present in other gymnolaemates, but disappears during ontogeny (Weber et al., 2014) and was not observed in any other adult zooid of myolaemate species. The structure of the cyclostome cerebral ganglion corresponds to that of gymnolaemates except for the presence of two lateral lobes associated with the ganglion, as shown in *Crisiidia cornuta* (Lutaud, 1979b) and recent studies in *Crisia eburnea* (Temereva & Kosevich, 2018), and *Cinctipora elegans* (Schwaha et al., 2018). The cerebral ganglia of phylactolaemates are characteristically croissant shaped fluid filled vesicles and have two lateral extensions in the form of so-called ganglionic horns (Gruhl & Bartolomaeus, 2008; Shunkina et al., 2015; Ambros et al., 2018). The ganglionic horns are nervous masses that extend in the lophophoral arms (Gruhl & Schwaha, 2015).

The most prominent neurite bundle emanating from the cerebral ganglion is a circumoral nerve ring, which occurs in all bryozoan taxa (Lutaud, 1969; Schwaha & Wanninger, 2015; Shunkina et al., 2015; Temereva & Kosevich, 2016; Ambros et al., 2018; Schwaha et al., 2018). The thick nerve ring gives rise to the tentacle neurite bundles in cheilostomes (Figs. 11, 12, 13, 14, 15, 16). This is also true for myolaemates (Schwaha et al., 2020; Schwaha, in press). The situation in phylactolaemates is similar but the majority of tentacle neurite bundles of this taxon emanate from the ganglionic horns (Gruhl & Bartolomaeus, 2008; Shunkina et al., 2015; Ambros et al., 2018). They are a necessary adaption to the horseshoe shape of the lophophore and the high number of tentacles in this taxon (Gruhl & Bartolomaeus, 2008; Shunkina et al., 2015; Ambros et al., 2018). In the miniaturized phylactolaemate *Fredericella sultana* lophophoral arms are absent and ganglionic horns are almost entirely lost (Shunkina et al., 2015). As result tentacle neurite bundles emanate solely from the circumoral nerve ring in *F. sultana* (Shunkina et al., 2015).

4.2 Tentacle sheath innervation

Two direct tentacle sheath neurite bundles emanate from the anal side of the cerebral ganglion of all examined species (Figs. 3D, 4D, 5D, 7D, 14A, 16A). In the cheilostome *Electra pilosa* (Lutaud, 1969) and the ctenostomes *Alcyonidium polyoum* (Bronstein, 1937), *Amathia gracilis* (Temereva & Kosevich, 2016) and *Farrella repens* (Marcus,

14

1926) two perikarya were described in this area. Corresponding perikarya were not found in this study. In cyclostomes, a similar pair of tentacle sheath neurite bundles emanate from the cerebral ganglion (Schwaha et al., 2018). The tentacle sheath of phylactolaemates is innervated via a diffuse plexus that extends to the body wall via the vestibular wall (Gerwerzhagen, 1913; Gruhl & Bartolomaeus, 2008; Gruhl & Schwaha, 2015; Shunkina et al., 2015; Ambros et al., 2018). In this group four distinct neurite bundles emanate from the cerebral ganglion and circumoral nerve ring, two on the oral and two on the anal side, and partly give rise to the plexus (Shunkina et al., 2015; Ambros et al., 2018).

The trifid neurite bundles project laterally and bend towards the vestibular wall in a right angle (Fig. 3D-8D). They generally have three branches: (1) main branches fuse with the direct tentacle sheath neurite bundles, (2) proximal branches innervate parts of the retractor muscle and gut, and (3) annular branches surround the lophophore proximally in form of an open ring (Fig. 3D-8D). A similar structure of the trifid neurite bundles was found in other gymnolaemates (Graupner, 1930; Bronstein, 1937; Lutaud, 1969, 1976; Weber et al., 2014; Temereva & Kosevich, 2016; Pröts et al., 2019). The annular branch is absent in the cheilostome *Chartella papyracea* (Lutaud, 1976) and also in three species analyzed in this study (Tab. 2). The species *Chorizopora brongniartii*, *Collarina balzaci* and *Fenestrulina joannae* lack the annular branch of the trifid neurite bundles (Fig. 4A, 7A, 8A). They have distinctly smaller polypides than *Bugula neritina*, *Electra posidoniae* and *Myriapora truncata* (Fig. 3A-8A). It might be possible that the annular branches are absent due to miniaturization of the respective taxa. The direct tentacle sheath neurite bundles and trifid neurite bundles always fuse to compound tentacle sheath neurite bundles in cheilostomes (Figs. 3D, 4D, 5D, 6D, 7D, 8D), which corresponds to early findings in the cheilostome *Membranipora membranacea* (Marcus, 1926) and the ctenostome *Flustrellidra hispida* (Marcus, 1926; Graupner, 1930). The two neurite bundles project in parallel in *Electra pilosa* where they correspond in terms of location to the fused compound tentacle sheath neurite bundles (Lutaud, 1969). In the ctenostome neurite bundles neurite bundles rifid neurite bundles are absent in cyclostomes and phylactolaemates they could be an apomorphy of gymnolaemates.

In the ctenostome species *Amathia gracilis* and the cyclostomes *Cinctipora elegans* and *Crisia eburnea,* an outer nerve ring was identified (Temereva & Kosevich, 2016;

Schwaha et al., 2018; Temereva & Kosevich, 2018). It forms a full outer circle that is concentric to the circumoral nerve ring (Temereva & Kosevich, 2016; Schwaha et al., 2018; Temereva & Kosevich, 2018). The outer ring nerve is reported as mostly incomplete in *C. elegans* (Schwaha et al., 2018). It emanates from the lateral parts of the trifid neurite bundles in the ctenostome *A. gracilis* (Temereva & Kosevich, 2016). A corresponding neurite bundle exists in the ctenostome *Paludicella articulata* (Weber et al., 2014). In this species, the structure was not identified as part of the outer nerve ring in the first place and interpreted as such in a subsequent study of *C. elegans* (Schwaha et al., 2018). While the outer nerve ring is fully present in *A. gracilis* (Temereva & Kosevich, 2016) and at least partly present in *P. articulata* (Weber et al., 2014), it is absent in the ctenostome *Hypophorella expansa* (Pröts et al., 2019) and in cheilostomes. It is fully present in cyclostomes (sister-group of gymnolaemates) and absent in phylactolaemates. The outer nerve ring may thus represent an apomorphy of myolaemates, together with their triradiate muscular pharynx. In this taxon, the innervation of peripheral structures was centralized to major neurite bundles, rather than utilizing a diffuse plexus as found in phylactolaemates. Alternatively, the outer nerve ring could be lost in phylactolaemates and represent an apomorphy of bryozoans.

4.3 **Visceral innervation**

The visceral innervation consists of five neurite bundles that project towards the digestive tracts of *Bugula neritina*, *Electra posidoniae* and *Myriapora truncata* (Figs. 6D, 11A, 13A, 14A). One central, mediovisceral neurite bundle projects from the cerebral ganglion towards the proximal end of the pharynx on its anal side and terminates at the cardia (Figs. 3D, 4D, 5D, 6C, 7D, 8B). The origin of its neurites can be traced back to distinct somata at the proximal end of the ganglion as shown in the cheilostome *Electra pilosa* (Lutaud, 1969). In *Chorizopora brongniartii*, *Collarina balzaci* and *Fenestrulina joannae* mediolaterovisceral neurite bundles are absent and only three neurite bundles innervate the pharynx (Tab. 2). The pharynx as most prominent muscular structure in the cheilostome visceral tract has additional motoric innervation that originates from the trifid neurite bundles (Graupner, 1930; Lutaud, 1969). This study identified descending branches of the trifid neurite bundles as remnants of the outer nerve ring that correspond to the respective structures (Fig. 9, Tab. 2). The visceral neurite bundles are connected by a pharyngeal nerve plexus,

which is absent only in *C. brongniartii* (Tab. 2). Regarding ctenostomes, the pharynx of *Paludicella articulata* is innervated by six to eight neurite bundles (Weber et al., 2014). A medio- and two laterovisceral neurite bundles are always present in this species while the number of mediolaterovisceral neurite bundles varies between two to four (Weber et al., 2014). Similarly, numerous neurite bundles were identified in *Amathia gracilis* and *Hypophorella expansa* (Temereva & Kosevich, 2018; Pröts et al., 2019). Due to the lack of a ctenostome phylogeny (the sister group to cheilostomes) the visceral innervation pattern of gymnolaemates cannot yet be resolved. The gut of the cyclostome *Cinctipora elegans* is innervated by four neurite bundles, which closely resembles the pattern described in cheilostomes (Schwaha et al., 2018). However, studies of *Crisia eburnea* indicate variable numbers of visceral neurite bundles and plexus like innervation in cyclostomes (Temereva & Kosevich, 2018; Worsaae et al., 2018). The visceral innervation of phylactolaemates extends over the pharynx to the cardia as a plexus with two prominent neurite bundles (Shunkina et al., 2015; Ambros et al., 2018). In *Hyalinella punctata,* the plexus of phylactolaemates is denser around the pharynx than the cardia (Ambros et al., 2018). The pharyngeal nerve plexus could be present at the base of bryozoans and concentrated to numerous neurite bundles in cyclostomes and ctenostomes. In this case, these neurite bundles would have fused or part of them was lost to represent the innervation pattern present in gymnolaemates. This question can only be clarified by investigations of phoronids, the sister group of Bryozoa (Laumer et al., 2019; Marlétaz et al., 2019). To date, there were no studies on the visceral innervation of this group.

4.4 Peripheral innervation

In cheilostomes the compound tentacle sheath neurite bundles project along the duplicature bands, where they split at a parietal branching point in the prevestibular area to innervate aperture associated- and parietal musculature (Figs. 3C-7C). In contrast to findings in *E. pilosa* where neurite bundles branch off the compound tentacle sheath neurite bundle from different locations (Lutaud, 1973a), this study found one branching point from where all aperture associated muscles are innervated in cheilostomes (Figs. 3E, 4E, 5E, 7E, 8E). The peripheral innervation pattern of cheilostomes also corresponds to that of the ctenostome *Paludicella articulata* (Weber et al., 2014). Only the direct tentacle sheath neurite bundles (not fused with the trifid component) give rise to the corresponding aperture associated neurite bundles in the

ctenostome *Hypophorella expansa* (Pröts et al., 2019). The innervation of peripheral areas via only the direct tentacle sheath neurite bundles in *H. expansa* corresponds to that found in the cyclostomes *Cinctipora elegans* and *Crisia eburnea* (Schwaha et al., 2018; Temereva & Kosevich, 2018). In phylactolaemates, aperture associated muscles are innervated via the diffuse nervous plexus of the tentacle sheath that originates from two to four major neurite bundles emanating from the cerebral ganglion and the circumoral nerve ring (Ambros et al., 2018).

Parietal muscles are innervated via a neurite bundle that branches off the operculum occlusor neurite bundle and also innervates parts of the frontal wall in *Electra pilosa* (Lutaud, 1973b). The branch innervating the frontal wall of *E. pilosa* was referred to as axial residual branch and presumably terminates in spines of the cystid (Lutaud, 1973a). While the parietal muscle neurite bundle is verified by the present study (Fig. 3E, 4E, 6C, 7E, 8E), no additional branch terminating in the frontal wall was identified. This is similar in the cheilostome *Chartella papyracea* (Lutaud, 1976). The identification of the parietal neurite bundle as a single structure in cheilostomes (Fig. 3E, 4E, 6C, 7E, 8E) corresponds to findings in the cheilostome *Membranipora membranacea* (Marcus, 1926) and the ctenostome *Alcyonidium gelatinosum* (Bronstein, 1937), supporting a common gymnolaemate pattern. The parietal muscle neurite bundles are absent in cyclostomes and phylactolaemates due to the different protrusion methods of the taxa. Annular muscles around the membranous sac of cyclostomes are innervated via fine neurite bundles in the epithelial lining of diagonal and circular muscles of the membranous sac, as shown in *Cinctipora elegans* and *Crisia eburnea* (Schwaha et al., 2018; Temereva & Kosevich, 2018). Accordingly, they form a net of longitudinal and transversal neurite bundles around the membranous sac (Temereva & Kosevich, 2018). In *C. eburnea*, additional ectodermal body wall muscles were identified that aid the increase of pressure in the body cavity for the purpose of polypide protrusion (Worsaae et al., 2018). While their innervation was not regarded in the first place, a later study found that they are innervated by distinct neurite bundles that are in contact with a ring nerve surrounding the diaphragmatic sphincter and the outer nerve ring (Temereva & Kosevich, 2018). Similar muscles were not found in other cyclostomes. The orthogonal body wall musculature of phylactolaemates is innervated via two of the two to four neurite bundles that innervate the tentacle sheath (Gruhl & Bartolomaeus, 2008; Ambros et al., 2018 ; Schwaha et al., 2020). The respective

neurite bundles project along the duplicature bands before they split (Gruhl & Bartolomaeus, 2008; Ambros et al., 2018).

The neurite bundle innervating the diaphragmatic sphincter splits in two parts that form a ring in *Electra posidoniae* (Fig. 3E), which corresponds to descriptions in *Electra pilosa* (Lutaud, 1973b). A similar innervation of the diaphragmatic sphincter was identified in the cyclostome *Crisia eburnea* (Temereva & Kosevich, 2018). Generally, in cheilostomes this muscle is not innervated via a ring but via two distinct neurite bundles innervating the muscle from the lateral sides (Figs. 4E, 5E, 6C, 7E, 8E). The situation observed in the genus *Electra* is possibly an apomorphy of malacostegan cheilostomes. No information is available on the detailed innervation of the diaphragmatic sphincter muscle of ctenostomes. In the cyclostomes *Crisiidia cornuta* (Lutaud, 1979b) and *Cinctipora elegans* (Schwaha et al., 2018) a vestibular branch innervates the diaphragmatic sphincter muscle with branches spreading into the vestibular wall.

Cheilostome opercular neurite bundles always terminate at the respective operculum occlusor muscles (Figs. 3D, 4D, 5D, 7D, 8D). In *Electra pilosa*, the opercular branches innervate the opercular muscles from the lateral sides and connect to each other distally at the basal side of the zooid, to form a circular structure (Lutaud, 1973a). This situation could not be verified in the present study. There are, however, small processes on the opercular neurite bundles of *Electra posidoniae* and *Collarina balzaci* that are topologically similar to the described structures (Fig. 3E, 7E). Since operculum occlusor muscles of cheilostomes are homologous to parietovestibular muscles of ctenostomes (Schwaha et al., 2011), a homologue of the opercular neurite bundle might be present in ctenostomes but has not been described to this date.

Little information is available on the innervation of heterozooids and only few species of the genus *Bugula* were investigated (Lutaud, 1977b). Vital staining experiments revealed avicularia, defending zooids, possess their own "heterozooidal" nervous systems (Lutaud, 1977b). It is unknown how heterozooids communicate with the remaining colony. The structure responsible for zooidal communication is a nervous plexus called Hiller's plexus, located in the cystid wall (Hiller, 1939; Lutaud, 1969, 1979a, 1982b). This plexus originates from two separate neurite bundles that emanate from the proximal basal area of the cerebral ganglion close to the direct tentacle sheath neurite bundles and has nuclear nodes (Lutaud, 1969, 1979a). Plexi of adjacent zooids

are associated with interzooidal pores (Lutaud, 1977a). The plexus was shown in the cheilostomes *Electra pilosa* (Hiller, 1939; Lutaud, 1969) and *Membranipora membranacea* (Hiller, 1939) and the ctenostomes *Alcyonidium polyoum* (Lutaud, 1981) and *Amathia gracilis* (Lutaud, 1974). It was later subject to a transmission electron microscopical study that found that the plexus consists of single neurites lying in between the epithelium and the peritoneum (Lutaud, 1977a). Since no neural connections between zooids were found apart from Hiller's plexus, it remains the most probable mode of zooidal communication. No structure corresponding to or associated with Hiller's plexus was found in the present study or any other recent studies employing ICC analyses. Methylene blue vital staining proves to be a problematic method that needs to be reestablished. Transmission electron microscopy should be reemployed next in future studies of Hiller's plexus. A second structure that could be associated with colonial coordination is the funicular system. The cheilostome funicular system is known to transport and store metabolites (Lutaud, 1977a, 1982a; Schwaha et al., 2020). It is attributed to serve a double function in colonial coordination (Lutaud, 1982b). It is, however, not innervated and serves primarily as a reservoir to make nutrients available for zooids renewing their polypides or generating buds (Lutaud, 1982a).

4.5 **Tentacular innervation**

In cheilostomes, each tentacle is innervated by four neurite bundles (Figs. 9B, 17). One mediofrontal, two laterofrontal and one abfrontal tentacle neurite bundle are present in each tentacle in all bryozoan taxa (Schwaha, in press). This is a characteristic gymnolaemate pattern since it is also found in the ctenostomes *Amathia gracilis* (Temereva & Kosevich, 2016), *Hypophorella expansa* (Pröts et al., 2019) and *Paludicella articulata* (Weber et al., 2014). As only exception, six tentacle nerves were described in the cheilostome *Cryptosula pallasiana* (Gordon, 1974). The two additional nerves in this species are subperitoneal neurites (Gordon, 1974). Concerning cyclostomes, four tentacle neurite bundles were found in *Cinctipora elegans* (Schwaha et al., 2018), whereas six are present in *Crisia eburnea* (Temereva & Kosevich, 2018; Worsaae et al., 2018). The two additional neurite bundles in the latter species do not extend over the full length of the tentacle and terminate in sensory endings (Worsaae et al., 2018). In phylactolaemates, six neurite bundles innervate each tentacle (Ambros et al., 2018). The two additional neurite bundles extend over the tentacles as

20

lateroabfrontal neurite bundles (Shunkina et al., 2015; Ambros et al., 2018; Schwaha et al., 2020).

In cheilostomes, mediofrontal tentacle neurite bundles emanate directly from the circumoral nerve ring or the cerebral ganglion via two small rootlets (Figs. 9B, 17). A similar situation is found in ctenostomes (Weber et al., 2014; Temereva & Kosevich, 2018; Pröts et al., 2019). In cyclostomes the mediofrontal neurite bundle is also a fusion product of two neurite bundles (Temereva & Kosevich, 2018). In *Cinctipora elegans* mediofrontal tentacle neurite bundles were reported to connect to laterofrontal tentacle neurite bundles (Schwaha et al., 2018). Similar connections were not found in other species before. In phylactolaemates, the mediofrontal neurite bundles branch off proximal parts of radial neurite bundles that give rise to multiple neurite bundles (Shunkina et al., 2015; Ambros et al., 2018).

The remaining tentacle neurite bundles, namely two laterofrontal and one abfrontal neurite bundle, emerge from radial neurite bundles that emanate directly from the circumoral nerve ring and brain in cheilostomes (Fig. 17). In *Electra pilosa* the radial neurite bundles emanate from the circumoral nerve ring, but only give rise to two laterofrontal neurite bundles, each innervating adjacent tentacles (Lutaud, 1973b). In *E. pilosa*, the abfrontal neurite bundles emanate directly from the circumoral nerve ring or from the cerebral ganglion (Lutaud, 1973b). This study proves that abfrontal neurite bundles emanate via a single root from the radial neurite bundles around the circumoral nerve ring and possess two roots in the tentacles close to the cerebral ganglion (Fig. 9B). Correspondingly, they were reported to form separate roots close to the cerebral ganglion in the cyclostome *Cinctipora elegans* (Schwaha et al., 2018). Potential sensory cells on the tentacle tips of *Electra pilosa* and *Membranipora membranacea* (Lutaud, 1993) could not be identified in this study, but were found in the cheilostome *Bicellariella ciliata* (Schwaha & Wanninger, 2015) and the ctenostome *Flustrellidra hispida* (Graupner, 1930). These reports and the presence of ciliary tufts on the abfrontal side of the tentacles provide support for the sensory nature of abfrontal tentacle neurite bundles (Schwaha & Wanninger, 2015).

Radial neurite bundles are present in all bryozoan taxa (Schwaha et al., 2020; Schwaha, in press) and terminate in intertentacular sites in cheilostomes (Figs. 9B, 17). In all gymnolaemate bryozoans examined so far, intertentacular pits are located between adjacent tentacles (Lutaud, 1993; Weber et al., 2014; Schwaha & Wanninger,

2015; Temereva & Kosevich, 2016). The intertentacular sites found in the present study correspond to intertentacular perikarya, located in intertentacular pits of gymnolaemates (Lutaud, 1993; Weber et al., 2014; Schwaha & Wanninger, 2015; Temereva & Kosevich, 2016). Corresponding intertentacular perikarya were found in *Electra pilosa* and *Membranipora membranacea* and were interpreted as strain receptors by their cytoskeleton and the bearing of microvilli at a swollen ending (Lutaud, 1993). In eight ctenostome and thirteen cheilostome species, a characteristic pattern of serotonin expression in intertentacular perikarya was found (Schwaha & Wanninger, 2015).

Intertentacular bases were described in one cyclostome species, *Cinctipora elegans* and resemble intertentacular pits, except that they are solid epidermal cone shaped structures rather than pits as in gymnolaemates (Schwaha et al., 2018). In phylactolaemates, intertentacular perikarya exist (Ambros et al., 2018), but associated pits were not described. From the intertentacular sites of cheilostomes, neurites reach into the intertentacular pits (Fig. 17), where they probably serve sensory functions. Intertentacular neurites were found also in the ctenostome *Amathia gracilis* (Temereva & Kosevich, 2016). The neurites are not serotonergic (Schwaha & Wanninger, 2015).

4.6 Potential of complementary methods in neuroanatomical research

Methylene blue vital staining was used as state-of-the-art neuroanatomical method in early bryozoology research (Gerwerzhagen, 1913; Graupner, 1930; Bronstein, 1937; Lutaud, 1969). It was established in vertebrate histology and can provide details that could not be visualized with any method before the invention of ICC and CLSM (Ehrlich, 1886; Ramón y Cajal, 1894). Major difficulties of the method were always durability of samples and staining that was restricted to parts of specimens (Ehrlich, 1886; Aescht et al., 2015). Correspondingly, bryozoologists who used this method reported that only parts of the polypides were stained by the dye in most cases (Gerwerzhagen, 1913; Graupner, 1930; Lutaud, 1969). Additionally, the method is less efficient than ICC in combination with CLSM. Methylene blue vital staining is, however, the only method that labelled Hiller's plexus (Hiller, 1939; Lutaud, 1974, 1979b, 1981). It might be essential to reestablish this method to gain insight into the structure of Hiller's plexus. In the experiments conducted in this study, the methylene blue spread diffusely in the tissues of the samples in all experiments. Since methylene blue stains negatively charged structures, this diffuse staining could be due to changes in the

22

internal charge of the neurons in the live animals. When an action potential passes along the cell membrane of a neuron the internal charge of the cell changes from negative to positive. This might prevent labelling with the dye or remove already labelled cell components. Anesthetizing the specimens prior to the experiment could help to keep the dye in the neurons until documentation. To ease the reestablishment of a protocol it will be helpful to conduct experiments in a large bryozoan species such as *Cristatella mucedo* and then adapt a working protocol for large marine and later smaller marine species.

Silver staining of the nervous system is less problematic than methylene blue vital staining and provides durable samples. Thus, both methods were frequently used in combination by bryozoologists (Lutaud, 1977a). The species *Electra pilosa* was especially well investigated using silver staining (Lutaud, 1973b, 1973a). In contrast to methylene blue vital staining, various protocols were established for this method (Strausfeld, 1980; Metscher, 2009; Aescht et al., 2015). Recently, the method shed light on the organizations of brains of different terrestrial and marine arthropods that were mainly examined by serial sectioning of the specimens (Strausfeld, 1970; Ignell et al., 2005; Ignell & Hansson, 2005; Strausfeld, 2005; Sztarker et al., 2005; Sombke et al., 2011; Krieger et al., 2019). No studies were recently conducted in lophotrochozoans with this method. A major potential of the method lies in a combination with micro computed tomography (μCT). The μCT method has yielded positive results in vertebrates (Dorr et al., 2007; Aggarwal et al., 2009; Mizutani & Suzuki, 2012), arthropods (Fanenbruck et al., 2001; Wirkner & Richter, 2004; Tanisako et al., 2005; Wirkner & Prendini, 2007; Friedrich & Beutel, 2008; Ribi et al., 2008; Sombke et al., 2015; Lehmann & Melzer, 2018; Sombke et al., 2019), and some marine invertebrates (Henne et al., 2017; Beckers et al., 2019). Silver staining combined with μCT could innovate bryozoan neuroanatomical research especially by the yield of clear whole mount imaging. Studies of nematomorphs and annelids show that the incubation with iodine or phosphotungstic acid are promising alternatives to inspect bryozoans with μCT (Henne et al., 2017; Beckers et al., 2019).

Neuronal tracing with DiI allows tracing single neurons and gain information about synaptic connections of neurons, which is the major potential of this method. It was used in vertebrates (Linke & Frotscher, 1993; Zullo & Hochner, 2011) and invertebrates (Stemme et al., 2014) and is compatible with other ICC methods (Von Bartheld et al.,

1990; Matsubayashi et al., 2008). It is not yet established for small animals like bryozoan zooids. The method could make the examination of small features like tentacular neurite bundles especially easy. In this study's experiments, the tracer labelled caecum ligaments and the surrounding tissues of the digestive tract (Fig. 18). This shows clearly that all damaged cells in contact with the tracer were infiltrated, regardless of their tissue type (Fig. 18). The method is regarded unsuitable for small species in which the tracer cannot be applied to specific structures, until an application mode is available that can take reasonable amounts of DiI to the application sites to prevent overstaining of tissues.

ICC reveals clear and precise results in short time. The specificity of this method lies in the choice of the primary antibody. The method is used for histological sections of all metazoan tissues and provides the possibility to design antibodies as markers against any cell component desired. Small animals as bryozoans can even be examined as whole mounts. In bryozoan neuroanatomical research, antibodies against (tyrosinated/acetylated) α-tubulin (Shunkina et al., 2013; Weber et al., 2014; Temereva & Kosevich, 2016; Ambros et al., 2018; Temereva & Kosevich, 2018; Worsaae et al., 2018; Pröts et al., 2019) and serotonin (Schwaha et al., 2011; Schwaha & Wanninger, 2012; Shunkina et al., 2013; Schwaha & Wanninger, 2015; Shunkina et al., 2015; Serova et al., 2016) were commonly used. Antibodies against FMRF-amide (Shunkina et al., 2015; Serova et al., 2016) are less frequently used, DLamide and RYamide were only used in an exploratory study that aimed to find conserved neuropeptides (Conzelmann & Jékely, 2012). Labelling of rarely targeted catecholaminergic cells revealed possible receptors in the epithelium of the freshwater bryozoan *Cristatella mucedo* (Shunkina et al., 2014; Shunkina et al., 2015). Anti-acetylated α-tubulin labelling provides a clear picture of the entire nervous system of bryozoans, but α-tubulin is also present in cilia of the tentacles and the digestive tract (Figs. 3- 8, 11-17). Anti-serotonin labelling showed serotonin expression among specific sites in the bryozoan polypide (Schwaha & Wanninger, 2015; Worsaae et al., 2018).

Concerning data collected in the present study, results line up well with the detailed results from previous studies using methylene blue vital staining and silver staining (Lutaud, 1969, 1973b). A complementary labelling of acetylated α-tubulin like structures and nervous system associated cell other than components, serotonin is recommendable for future studies. To explore less identified structures like Hiller's

24

plexus, it is recommendable to try different antibodies such as against γ-aminobutryc acid, which can shed light on inhibitory pathways.

Conclusion

This study provides data of the least investigated, yet biggest bryozoan taxon collected with state-of-the-art methods. It presents a broad overview on the nervous system of cheilostomes. The structure of the cerebral ganglion, visceral-, peripheral- and tentacular innervation are uniform in cheilostomes that vary only slightly within gymnolaemates. The presence of lateral areas in the cerebral ganglion as well as varying number of tentacle neurite bundles and tentacle sheath innervation supports the position of cyclostomes in Stenolaemata, the sister group to gymnolaemates. Major differences occurring between Myolaemata and Phylactolaemata lie in the structure of the cerebral ganglion, plexus-like innervation of the tentacle sheath and body wally and tentacular innervation in phylactolaemates. These differences suggest phylactolaemates at the base of Bryozoa. There is a high potential in the use of complementary methods in Bryozoa, as different methods are best to visualize different structures in the polypide and in the colony.

Acknowledgements

References

Aescht, E., Büchl-Zimmermann, S., Burmester, A., Dänhardt-Pfeiffer, S., Desel, C., Chamers, C., . . . Welsch, U. (2015). Romeis Mikroskopische Technik. In M. Mulisch & U. Welsch (Eds.), (Vol. 19). Heidelberg: Spektrum Akademischer Verlag.

Aggarwal, M., Zhang, J., Miller, M. I., Sidman, R. L., & Mori, S. (2009). Magnetic resonance imaging and micro-computed tomography combined atlas of developing and adult mouse brains for stereotaxic surgery. *Neuroscience, 162*(4), 1339-1350.

Ambros, M., Wanninger, A., & Schwaha, T. F. (2018). Neuroanatomy of *Hyalinella punctata*: common patterns and new characters in phylactolaemate bryozoans. *Journal of morphology, 279*(2), 242-258.

Beckers, P., Helm, C., Purschke, G., Worsaae, K., Hutchings, P., & Bartolomaeus, T. (2019). The central nervous system of Oweniidae (Annelida) and its implications for the structure of the ancestral annelid brain. *Frontiers in zoology, 16*(1), 6.

Bronstein, G. (1937). Étude du système nerveux de quelques Bryozaires Gymnolémides. *Travail Station Biologique de Roscoff, 15*, 155-174.

Conzelmann, M., & Jékely, G. (2012). Antibodies against conserved amidated neuropeptide epitopes enrich the comparative neurobiology toolbox. *Evodevo, 3*(1), 23.

Dorr, A., Sled, J. G., & Kabani, N. (2007). Three-dimensional cerebral vasculature of the CBA mouse brain: a magnetic resonance imaging and micro computed tomography study. *Neuroimage, 35*(4), 1409-1423.

Ehrlich, P. (1886). Ueber die Methylenblaureaction der lebenden Nervensubstanz. *Deutsche Medizinische Wochenschrift, 12*(04), 49-52.

Fanenbruck, M., De Carlo, F., & Mancini, D. (2001). Evaluating the advantage of X-ray microtomography in microanatomical studies of small arthropods. *APS Activity Reports. Argonne, IL: Argonne National Laboratory*.

Friedrich, F., & Beutel, R. G. (2008). *Micro-computer tomography and a renaissance of insect morphology.* Paper presented at the Developments in X-ray tomography VI.

Gawin, N., Wanninger, A., & Schwaha, T. (2017). Reconstructing the muscular ground pattern of phylactolaemate bryozoans: first data from gelatinous representatives. *BMC Evolutionary biology, 17*(1), 225.

26

Gerwerzhagen, A. (1913). Beiträge zur Kenntnis der Bryozoen. 1 Das Nervensystem von *Cristatella mucedo* Cuv. *Zeitschrift für wissenschaftliche Zoologie, 107*, 309-345.

Gordon, D. P. (1974). Microarchitecture and function of the lophophore in the bryozoan *Cryptosula pallasiana. Marine Biology, 27*(2), 147-163.

Graupner, H. (1930). *Zur Kenntnis der feineren Anatomie der Bryozoen Nervensystem, Muskulatur, Stützmembran*. Leipzig: Akademische Verlagsgesellschaft.

Gruhl, A., & Bartolomaeus, T. (2008). Ganglion ultrastructure in phylactolaemate Bryozoa: Evidence for a neuroepithelium. *Journal of morphology, 269*(5), 594-603.

Gruhl, A., & Schwaha, T. F. (2015). Bryozoa (Ectoprocta). In A. Schmidt-Rhaesa, S. Harzsch, & G. Purschke (Eds.), *Structure and evolution of invertebrate nervous systems* (pp. 325-340). New York: Oxford University Press.

Hageman, S. J., Bock, P. E., Bone, Y., & McGowran, B. (1998). Bryozoan growth habits: classification and analysis. *Journal of Paleontology, 72*(3), 418-436.

Hayward, P. J., & Ryland, J. S. (1975). Growth, reproduction and larval dispersal in *Alcyonidium hirsutum* (Fleming) and some other Bryozoa. *Pubblicazioni della Stazione Zoologica, Napoli (Italy)*.

Henne, S., Friedrich, F., Hammel, J. U., Sombke, A., & Schmidt-Rhaesa, A. (2017). Reconstructing the anterior part of the nervous system of *Gordius aquaticus* (Nematomorpha, Cycloneuralia) by a multimethodological approach. *Journal of morphology, 278*(1), 106-118.

Hiller, S. (1939). The so-called "Colonial Nervous System" in Bryozoa. *Nature, 143*, 1069-1070.

Ignell, R., Dekker, T., Ghaninia, M., & Hansson, B. S. (2005). Neuronal architecture of the mosquito deutocerebrum. *Journal of Comparative Neurology, 493*(2), 207-240.

Ignell, R., & Hansson, B. S. (2005). Projection patterns of gustatory neurons in the suboesophageal ganglion and tritocerebrum of mosquitoes. *Journal of Comparative Neurology, 492*(2), 214-233.

Krieger, J., Hörnig, M. K., Sandeman, R. E., Sandeman, D. C., & Harzsch, S. (2019). Masters of communication: The brain of the banded cleaner shrimp *Stenopus hispidus* (Olivier, 1811) with an emphasis on sensory processing areas. *Journal of Comparative Neurology*.

Laumer, C. E., Fernández, R., Lemer, S., Combosch, D., Kocot, K. M., Riesgo, A., . . . Giribet, G. (2019). Revisiting metazoan phylogeny with genomic sampling of all phyla. *Proceedings of the royal society B, 286*(1906), 20190831.

Lehmann, T., & Melzer, R. R. (2018). Also looking like Limulus?–retinula axons and visual neuropils of Amblypygi (whip spiders). *Frontiers in zoology, 15*(1), 52.

Linke, R., & Frotscher, M. (1993). Development of the rat septohippocampal projection: tracing with DiI and electron microscopy of identified growth cones. *Journal of Comparative Neurology, 332*(1), 69-88.

Lutaud, G. (1969). Le «plexus» pariétal de Hiller et la coloration du système nerveux par le bleu de méthylène chez quelques Bryozoaires Chilostomes. *Zeitschrift für Zellforschung und mikroskopische Anatomie, 99*(2), 302-314.

Lutaud, G. (1973a). The great tentacle sheath nerve as the path of an innervation of the frontal wall structures in the cheilostome *Electra pilosa* (Linné). In G. P. Larwood (Ed.), *Living and fossil Bryozoa* (pp. 3l7-326). New York: Academic Press.

Lutaud, G. (1973b). L'innervation du lophophore chez le Bryozoaire chilostome *Electra pilosa* (L.). *Zeitschrift für Zellforschung und mikroskopische Anatomie, 140*(2), 217-234.

Lutaud, G. (1974). Le plexus parietal des cténostomes chez *Bowerbankia gracilis* Leydi (Vésicularines). *Cahiers de Biologie marine, 1974*, 403-408.

Lutaud, G. (1976). L'innervation des parois de la loge chez *Flustra papyracea* (Ellis et Solander) (Bryozoaire Chilostome). *Cahiers de Biologie marine, 17*, 337-346.

Lutaud, G. (1977a). The bryozoan nervous system. In R. Woollacott & R. Zimmer (Eds.), *Biology of bryozoans* (pp. 377-410). New York: Academic press, Inc.

Lutaud, G. (1977b). L'innervation de l'aviculaire pedoncule des Bicellariidae (Bryozoaires Chilostomes). *Cahiers de Biologie marine, 18*, 435-448.

Lutaud, G. (1979a). Etude ultrastructurale du "plexus colonial" et recherche de connexions nerveuses interzoidiales chez le bryozoaire chilostome *Electra pilosa* (Linné). *Cahiers de Biologie marine, 20*, 315-324.

Lutaud, G. (1979b). The probability of a plexus in the calcified wall of *Crisiidia cornuta* (Linné). In G. P. Larwood & M. B. Abbott (Eds.), *Advances in Bryozoology* (Vol. Systematics Association special volume 13, pp. 33-45). London & New York: Academic Press.

Lutaud, G. (1980). Étude morphologique et ultrastructurale de certaines cellules sensorielles de la paroi basale du Zoïde chez le Bryozoaire Chilostome *Electra pilosa* (L.). *Cahiers de Biologie marine, 21*, 91-98.

Lutaud, G. (1981). The innervation of the external wall in the carnosan ctenostome *Alcyonidium polyoum* (Hassall). In G. P. Larwood & C. Nielsen (Eds.), *Recent and fossil Bryozoa* (pp. 143-150). Fredensborg, Denmark: Olsen & Olsen.

Lutaud, G. (1982a). Étude morphologique et ultrastructurale du funicule lacunaire chez le Bryozoaire Chilostome *Electra pilosa* (Linné). *Cahiers de Biologie marine, 23*, 71-81.

Lutaud, G. (1982b). La communauté des parois et les voies de l'unité physiologique de la colonie chez les Bryozoaires Eurystomes. *Bulletin de la Sociètè Zoologique de France, 107*, 251-266.

Lutaud, G. (1993). *L'innervation sensorielle du lophophore et de la region orale chez les Bryozoaires Cheilostomes.* Paper presented at the Annales des Sciences Naturelles, Zoologie, Paris.

Marcus, E. (1926). Beobachtungen und Versuche an lebenden Meeresbryozoen. *Zoologische Jahrbücher Abteilung für Systematik, Ökologie und Geographie der Tiere, 52*, 1-102.

Marlétaz, F., Peijnenburg, K. T., Goto, T., Satoh, N., & Rokhsar, D. S. (2019). A new spiralian phylogeny places the enigmatic arrow worms among gnathiferans. *Current Biology, 29*(2), 312-318. e313.

Martha, S. O., Niebuhr, B., & Scholz, J. (2016). 9. Cheilostome Bryozoen. In B. Niebuhr & M. Wilmsen (Eds.), *Kreide-Fossilien in Sachsen* (Vol. 62, pp. 11-52): Geologica Saxonica.

Massard, J. A., & Geimer, G. (2008). Occurrence of *Plumatella emarginata* Allman, 1844 and *P. casmiana* Oka, 1908 (Bryozoa, Phylactolaemata) in Lake Pamvotis (Ioannina, Greece). *Bulletin de la Société des naturalistes luxembourgeois, 109*, 133-138.

Matsubayashi, Y., Iwai, L., & Kawasaki, H. (2008). Fluorescent double-labeling with carbocyanine neuronal tracing and immunohistochemistry using a cholesterol-specific detergent digitonin. *Journal of neuroscience methods, 174*(1), 71-81.

Metscher, B. D. (2009). MicroCT for comparative morphology: simple staining methods allow high-contrast 3D imaging of diverse non-mineralized animal tissues. *BMC physiology, 9*(1), 11.

Mizutani, R., & Suzuki, Y. (2012). X-ray microtomography in biology. *Micron, 43*(2-3), 104-115.

Mukai, H., Terakado, K., & Reed, C. G. (1997). Bryozoa. In F. Harrison & R. Woollacott (Eds.), *Microscopic anatomy of invertebrates* (Vol. 13, pp. 45-206). New York: Wiley-Liss.

Nielsen, C., & Pedersen, K. J. (1979). Cystid structure and protrusion of the polypide in *Crisia* (Bryozoa, Cyclostomata). *Acta Zoologica, 60*(2), 65-88.

Nielsen, C., & Riisgård, H. U. (1998). Tentacle structure and filter-feeding in *Crisia eburnea* and other cyclostomatous bryozoans, with a review of upstream-collecting mechanisms. *Marine Ecology Progress Series, 168*, 163-186.

Pröts, P., Wanninger, A., & Schwaha, T. (2019). Life in a tube: morphology of the ctenostome bryozoan *Hypophorella expansa. Zoological letters, 5*(1), 1-17.

Ramón y Cajal, S. (1894). Die Retina der Wirbelthiere: Untersuchungen mit der Golgi-Cajal'schen Chromsilbermethode und der Ehrlich'schen Methylenblaufärbung: Bergmann.

Ribi, W., Senden, T. J., Sakellariou, A., Limaye, A., & Zhang, S. (2008). Imaging honey bee brain anatomy with micro-X-ray-computed tomography. *Journal of neuroscience methods, 171*(1), 93-97.

Richter, S., Loesel, R., Purschke, G., Schmidt-Rhaesa, A., Scholtz, G., Stach, T., . . . Döring, C. (2010). Invertebrate neurophylogeny: suggested terms and definitions for a neuroanatomical glossary. *Frontiers in zoology, 7*(1), 29.

Riisgård, H. U., Okamura, B., & Funch, P. (2010). Particle capture in ciliary filter-feeding gymnolaemate and phylactolaemate bryozoans–a comparative study. *Acta Zoologica, 91*(4), 416-425.

Ryland, J. S. (1977). Physiology and ecology of marine bryozoans. In *Advances in marine biology* (Vol. 14, pp. 285-443): Elsevier.

Ryland, J. S. (2005). Bryozoa: an introductory overview. *Denisia, 16*(28), 9-20.

Schwaha, T. F. (in press). Morphology of Bryozoans. In T. F. Schwaha (Ed.), *Phylum Bryozoa*: unpublished draft.

Schwaha, T. F., Handschuh, S., Ostrovsky, A. N., & Wanninger, A. (2018). Morphology of the bryozoan *Cinctipora elegans* (Cyclostomata, Cinctiporidae) with first data on its sexual reproduction and the cyclostome neuro-muscular system. *BMC Evolutionary biology, 18*(1), 92.

Schwaha, T. F., Ostrovsky, A. N., & Wanninger, A. (2019). Key novelties in the evolution of the aquatic colonial phylum Bryozoa: evidence from soft body morphology. *Biological Reviews*.

Schwaha, T. F., Ostrovsky, A. N., & Wanninger, A. (2020). Key novelties in the evolution of the aquatic colonial phylum Bryozoa: evidence from soft body morphology. *Biological Reviews*.

Schwaha, T. F., & Wanninger, A. (2012). Myoanatomy and serotonergic nervous system of plumatellid and fredericellid Phylactolaemata (Lophotrochozoa, Ectoprocta). *Journal of morphology, 273*(1), 57-67.

Schwaha, T. F., & Wanninger, A. (2015). The serotonin-lir nervous system of the Bryozoa (Lophotrochozoa): a general pattern in the Gymnolaemata and implications for lophophore evolution of the phylum. *BMC Evolutionary biology, 15*(1), 223.

Schwaha, T. F., Wood, T. S., & Wanninger, A. (2011). Myoanatomy and serotonergic nervous system of the ctenostome *Hislopia malayensis*: evolutionary trends in bodyplan patterning of ectoprocta. *Frontiers in zoology, 8*(1), 11.

Serova, K. M., Vishnyakov, A. E., Zaitseva, O. V., & Ostrovsky, A. N. (2016). Distribution of serotonin and FMRF-amide in the nervous system of different zooidal types of cheilostome Bryozoa: a case study of *Arctonula arctica. Doklady Biological Sciences*, 471, 288-290.

Shunkina, K. V., Starunov, V. V., Zaitseva, O. V., & Ostrovsky, A. N. (2013). Serotonin and FMRFamide immunoreactive elements in the nervous system of freshwater bryozoans (Bryozoa: Phylactolaemata). *Doklady Biological Sciences, 451*(1), 244.

Shunkina, K. V., Zaitseva, O. V., Starunov, V. V., & Ostrovsky, A. N. (2015). Comparative morphology of the nervous system in three phylactolaemate bryozoans. *Frontiers in zoology, 12*(1), 28.

Shunkina, K. V., Zaytseva, O. V., Starunov, V. V., & Ostrovsky, A. N. (2014). Sensory elements and innervation in the freshwater bryozoan *Cristatella mucedo* lophophore*. Doklady Biological Sciences*, 455, 125.

Sombke, A., Harzsch, S., & Hansson, B. S. (2011). Organization of deutocerebral neuropils and olfactory behavior in the centipede *Scutigera coleoptrata* (Linnaeus, 1758)(Myriapoda: Chilopoda). *Chemical senses, 36*(1), 43-61.

Sombke, A., Klann, A. E., Lipke, E., & Wolf, H. (2019). Primary processing neuropils associated with the malleoli of camel spiders (Arachnida, Solifugae): a re-evaluation of axonal pathways. *Zoological letters, 5*(1), 1-13.

Sombke, A., Lipke, E., Michalik, P., Uhl, G., & Harzsch, S. (2015). Potential and limitations of X-Ray micro-computed tomography in arthropod neuroanatomy: A methodological and comparative survey. *Journal of Comparative Neurology, 523*(8), 1281-1295.

Stemme, T., Eickhoff, R., & Bicker, G. (2014). Olfactory projection neuron pathways in two species of marine Isopoda (Peracarida, Malacostraca, Crustacea). *Tissue and Cell, 46*(4), 260-263.

Strausfeld, N. J. (1970). Golgi studies on insects Part II. The optic lobes of Diptera. *Philosophical Transactions of the Royal Society of London. Series B, Biological Sciences, 258*(820), 135-223.

Strausfeld, N. J. (1980). The Golgi method: its application to the insect nervous system and the phenomenon of stochastic impregnation. In N. J. Strausfeld & T. A. Miller (Eds.), *Neuroanatomical techniques* (pp. 131-203). Heidelberg: Springer.

Strausfeld, N. J. (2005). The evolution of crustacean and insect optic lobes and the origins of chiasmata. *Arthropod structure & development, 34*(3), 235-256.

Sztarker, J., Strausfeld, N. J., & Tomsic, D. (2005). Organization of optic lobes that support motion detection in a semiterrestrial crab. *Journal of Comparative Neurology, 493*(3), 396-411.

Tanisako, A., Hori, A., Okumura, A., Miyata, C., Kuzuryu, C., Obi, T., & Yoshimura, H. (2005). Micro-CT of *Pseudocneorhinus bifasciatus* by projection X-ray microscopy. *Journal of electron microscopy, 54*(4), 379-383.

Temereva, E. N., & Kosevich, I. A. (2016). The nervous system of the lophophore in the ctenostome *Amathia gracilis* provides insight into the morphology of ancestral ectoprocts and the monophyly of the lophophorates. *BMC Evolutionary biology, 16*, 181.

Temereva, E. N., & Kosevich, I. A. (2018). The nervous system in the cyclostome bryozoan *Crisia eburnea* as revealed by transmission electron and confocal laser scanning microscopy. *Frontiers in zoology, 15*(1), 48.

Von Bartheld, C., Cunningham, D., & Rubel, E. (1990). Neuronal tracing with DiI: decalcification, cryosectioning, and photoconversion for light and electron

microscopic analysis. *Journal of Histochemistry & Cytochemistry, 38*(5), 725-733.

Waeschenbach, A., Taylor, P. D., & Littlewood, D. T. J. (2012). A molecular phylogeny of bryozoans. *Molecular Phylogenetics and Evolution, 62*(2), 718-735.

Weber, A. V., Wanninger, A., & Schwaha, T. F. (2014). The nervous system of *Paludicella articulata*-first evidence of a neuroepithelium in a ctenostome ectoproct. *Frontiers in zoology, 11*(1), 89.

Wirkner, C. S., & Prendini, L. (2007). Comparative morphology of the hemolymph vascular system in scorpions–A survey using corrosion casting, MicroCT, and 3D-reconstruction. *Journal of morphology, 268*(5), 401-413.

Wirkner, C. S., & Richter, S. (2004). Improvement of microanatomical research by combining corrosion casts with MicroCT and 3D reconstruction, exemplified in the circulatory organs of the woodlouse. *Microscopy Research and Technique, 64*(3), 250-254.

Worsaae, K., Frykman, T., & Nielsen, C. (2018). The neuromuscular system of the cyclostome bryozoan *Crisia eburnea* (Linnaeus, 1758). *Acta Zoologica*, 1-14.

Zabala, M., & Maluquer, P. (1988). *Treballs del Museu de Zoologia: Illustrated keys for the classification of Mediterranean Bryozoa* (O. Escolá, R. Nos, A. Omedes, & C. Prats i F. Uribe Eds. Vol. 4). Barcelona, Spain: Museu de Zoologia, Ajuntament de Barcelona.

Zullo, L., & Hochner, B. (2011). A new perspective on the organization of an invertebrate brain. *Communicative and integrative biology, 4*(1), 26-29.

Zusammenfassung

Bryozoen sind aquatische, sessile Filtrierer die sowohl marine als auch brackische Habitate bewohnen. Sie bilden Kolonien aus einer Vielzahl einzelner Individuen, genannt Zooide. Die meisten rezent vorkommenden Arten gehören zum Taxon Cheilostomata. Diese Gruppe besitzt unter anderem eine kalzifizierte Körperwand. Das Nervensystem dieser Gruppe ist wenig untersucht. Wesentliche morphologische Daten wurden mit Methylenblau Vitalfärbungen und Silberausfällung am Nervensystem der Tiere erhoben. Diese Methoden wurden später mit moderneren komplementiert. Der Fokus dieser Studie liegt auf der Charakterisierung und Analyse des autozooidalen Nervensystems cheilostomer Bryozoen. Die Analyse basiert auf Daten von sechs Arten aus fünf der wichtigsten Cheilostomata Taxa. Traditionelle und moderne Methoden wurden angewandt, um diese gegeneinander zu evaluieren. Dadurch soll zukünftige neuroanatomische Forschung an dieser, aber auch anderen Tiergruppen erleichtert werden. Die Ergebnisse zeigen ein gemeinsames Grundmuster im Nervensystem der untersuchten Gruppen. Das Zerebralganglion kommt an der Lophophorbasis zu liegen. Ein deutliches Nervenbündel umringt von dort die Mundöffnung als circumoraler Nervenring. Vier Nervenbündel ziehen vom Zerebralganglion Richtung distal um externe Muskeln wie etwa Parietal- und Operkulum Okklusor Muskeln durch die Tentakelscheide zu innervieren. Fünf Nervenbündel innervieren den Verdauungstrakt. Sie ziehen vom Gehirn entlang des Pharynx bis zur Cardia. Im übrigen Verdauungstrakt liegen keine deutlichen Nervenbündel. Die Tentakel der Tiere sind durch je vier Nervenbündel innerviert. Mediofrontale Tentakelnerven entspringen direkt vom circumoralen Nervenring. Die übrigen Nerven entspringen Radialnerven, die je zwischen zwei Tentakeln in intertentakuläre Gruben ragen. Pro Radialnerv ziehen zwei Laterofrontalnerven in die jeweils benachbarten Tentakel. Oralseitig entspringt jedem Radialnerv ein Abfrontalnerv, analseitig zwei. Diese Daten decken sich mit Forschungsergebnissen früherer Studien. Die gesammelten Daten formen die Basis einer Grundmuster-Analyse des cheilostomen autozooidalen Nervensystems. Ein ähnliches Muster findet sich in ctenostomem Bryozoen wodurch das hier beschriebene Muster auch Gymnolaemata zutrifft. Das Vorhandensein konzentrierter Neuritenbündel und Innervierung der Tentakel durch vier oder sechs Tentakelnerven unterstützt die Position von Cyclostomata als Intermediärtaxon zwischen Gymnolaemata und Phylactolaemata. Phylactolaemata besitzen wenige abgegrenzte Nervenbündel, die

sich je nach Innervierungsziel in der Tentakelscheide oder im Visceraltrakt in diffuse Nervenplexi teilen. Im Unterschied zu den anderen Gruppen haben Phylactolaemata immer sechs Tentakelnerven. Diese Unterschiede unterstützen Phylactolaemata als Schwestergruppe zu Myolaeamaten, den übrigen Bryozoa.

Tables and figures

Table 1: Identified bryozoan species, corresponding decalcification times in 20 % EDTA post fixation and applied staining techniques: Immunocytochemistry (ICC), methylene blue vital staining (MB) neuronal tracing with 1,1′-Dioctadecyl-3,3,3′,3′-tetramethylindocarbocyaninperchlorat (DiI) and silver staining (SI).

		Species	Growth pattern			EDTA	Techniques
"Anasca"	Flustrina	*Bugula neritina* (Linnaeus, 1758)	erect, thin branches			1h	ICC, SI
	Malacostega	*Electra posidoniae* Gautier, 1954	encrusting	on	*P. oceanica*	1h	ICC, DiI, SI, MB
"Ascophora"	Flustrina (Cribrimorpha)	*Collarina balzaci* (Audouin, 1826)	encrusting	on	*P. oceanica*	1h	ICC, SI
	Hippothoomorpha	*Chorizopora brongniartii* (Audouin, 1826)	encrusting	on	*P. oceanica*	1h	ICC, SI
	Lepraliomorpha	*Fenestrulina joannae* (Calvet, 1902)	encrusting	on	*P. oceanica*	1h	ICC, SI, MB
		Myriapora truncata (Pallas, 1766)	erect, massive branches			24h	ICC, SI, MB

Table 2: Nervous system character matrix. Characters have been analyzed for six species. From the 27 defined characters, 23 were used in the ground pattern analysis. Two characters were used in this matrix: present (1) and absent (0).

	Bugula neritina	*Chorizopora brongniartii*	*Collarina balzaci*	*Electra posidoniae*	*Fenestrulina joannae*	*Myriapora truncata*
lophophoral base						
cerebral ganglion	1	1	1	1	1	1
circumoral nerve ring	1	1	1	1	1	1
trifid nerve	1	1	1	1	1	1
descending branch	1	1	1	1	0	1
annular branch	1	0	0	1	0	1
direct nerve origin sites	0	0	0	0	0	0
direct tentacle sheath nerve	1	1	1	1	1	1
lophophore						
radial nerves	1	1	1	1	1	1
abfrontal tentacle nerve	1	1	1	1	1	1
mediofrontal tentacle rootlets	1	1	1	1	1	1
mediofrontal tentacle nerve	1	1	1	1	1	1
laterofrontal tentacle nerve	1	1	1	1	1	1
intertentacular sites	1	1	1	1	1	1
intertentacular neurites	1	1	1	1	1	1
visceral innervation						
mediovisceral nerve	1	1	1	1	1	1
laterovisceral nerves	1	1	1	1	1	1
mediolaterovisceral nerve	1	0	0	1	0	1
pharyngeal nerve plexus	1	0	1	1	1	1
visceral nerve origin site	0	0	0	0	0	0
peripheral innervation						
compound tentacle sheath nerve	1	1	1	1	1	1
parietal branching site	1	1	1	1	1	1
parietal muscle nerve	1	1	1	1	1	0
opercular branch	-	1	1	1	1	1
sphincter branch	1	1	1	1	1	1
parietodiaphragmatic nerve	1	1	1	1	1	1
remainder						
interzooidal pores	0	0	0	1	0	0

Table 3: Nervous system character matrix. Characters from previous studies have been evaluated after their manuscripts. Three character states were used in this matrix: present (1), absent (0) and missing data (?). All data except Marcus (1926) and Graupner (1930) originate from immunolabelling experiments using a primary antibody against acetylated α-tubulin. Marcus (1926) and Graupner (1930) used methylene blue vital staining.

Author	Temereva (2016) *Amanthia gracilis*	Marcus (1926) *Farrella repens*	Graupner (1930) *Flustrella hispida*	Schwaha (2011) *Hislopia malayensis*	Proets (2019) *Hypophorella expansa*	Weber (2011) *Paludecella articulata*
lophophoral base						
cerebral ganglion	1	1	1	1	1	1
circumoral nerve ring	1	1	1	1	1	1
outer nerve ring	1	?	?	?	0	0
trifid nerve	1	1	1	?	1	1
descending branch	?	?	1	?	?	?
annular branch	1	?	1	?	?	?
direct nerve origin sites	?	1	1	?	?	?
direct tentacle sheath nerve	1	1	1	?	1	1
lophophore						
radial nerves	1	?	?	1	1	1
abfrontal tentacle nerve	1	?	?	1	1	1
mediofrontal tentacle rootlets	1	?	?	?	1	1
mediofrontal tentacle nerve	1	?	?	1	1	1
laterofrontal tentacle nerve	1	?	?	1	1	1
intertentacular sites	1	?	?	1	?	?
intertentacular neurites	1	?	?	?	?	?
visceral innervation						
mediovisceral nerve	1	?	?	?	1	1
laterovisceral nerves	1	?	?	?	1	1
medio-laterovisceral nerve	1	?	?	?	?	1
pharyngeal plexus	1	?	?	?	1	1
visceral ganglion	?	?	?	?	?	?
visceral-lophophoral connection	?	?	?	?	?	?
peripheral innervation						
compound tentacle sheath nerve	?	?	1	?	?	?
parietal branching site	?	?	1	?	?	?
parietal muscle nerve	?	?	?	?	1	?
parietovestibular branch	?	?	?	?	?	?
sphincter branch	?	?	1	?	?	?
parietodiaphragmatic nerve	?	?	?	?	?	?
remainder						
interzooidal pores	?	?	?	?	?	?

Figure 1: Colony morphology of few cheilostome bryozoan species. **A** *Electra posidoniae* encrusting colony on *Posidonia oceanica*. **B** *Bugula neritina* erect dichotomous branching colony with biserial branches. **C** *Fenestrulina joannae* encrusting colony on *Posidonia oceanica*. **D** *Myriapora truncata* thick massive radial branch of irregularly branching colony. Abbreviations: **a** – ancestrula, **oc** – ovicell, **o** – operculum, **z** – zooid.
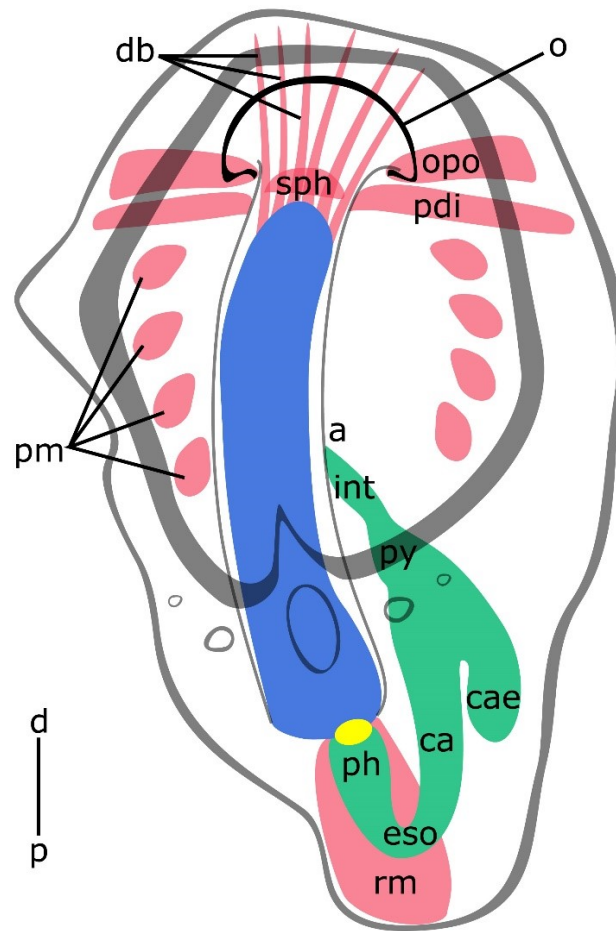
Figure 2: Schematic overview on the morphology of cheilostome bryozoans based on *Electra posidoniae* from frontal. The cystid (grey) is calcified. The polypide is composed of a lophophore (blue), digestive tract (green), musculature (pink) and the nervous system (cerebral ganglion in yellow). Digestive system modified from (Schwaha, in press). Abbreviations: **a** – anus, **cae** – caecum, **d** – distal, **db** – duplicature bands, **eso** – esophagus, **int** – intestine, **o** – operculum, **opo** – operculum occlusor muscle, **p** – proximal, **pdi** – parietodiaphragmatic muscle, **ph** – pharynx, **pm** – parietal muscle, **py** – pylorus, **rm** – retractor muscle, **sph** – sphincter muscle.
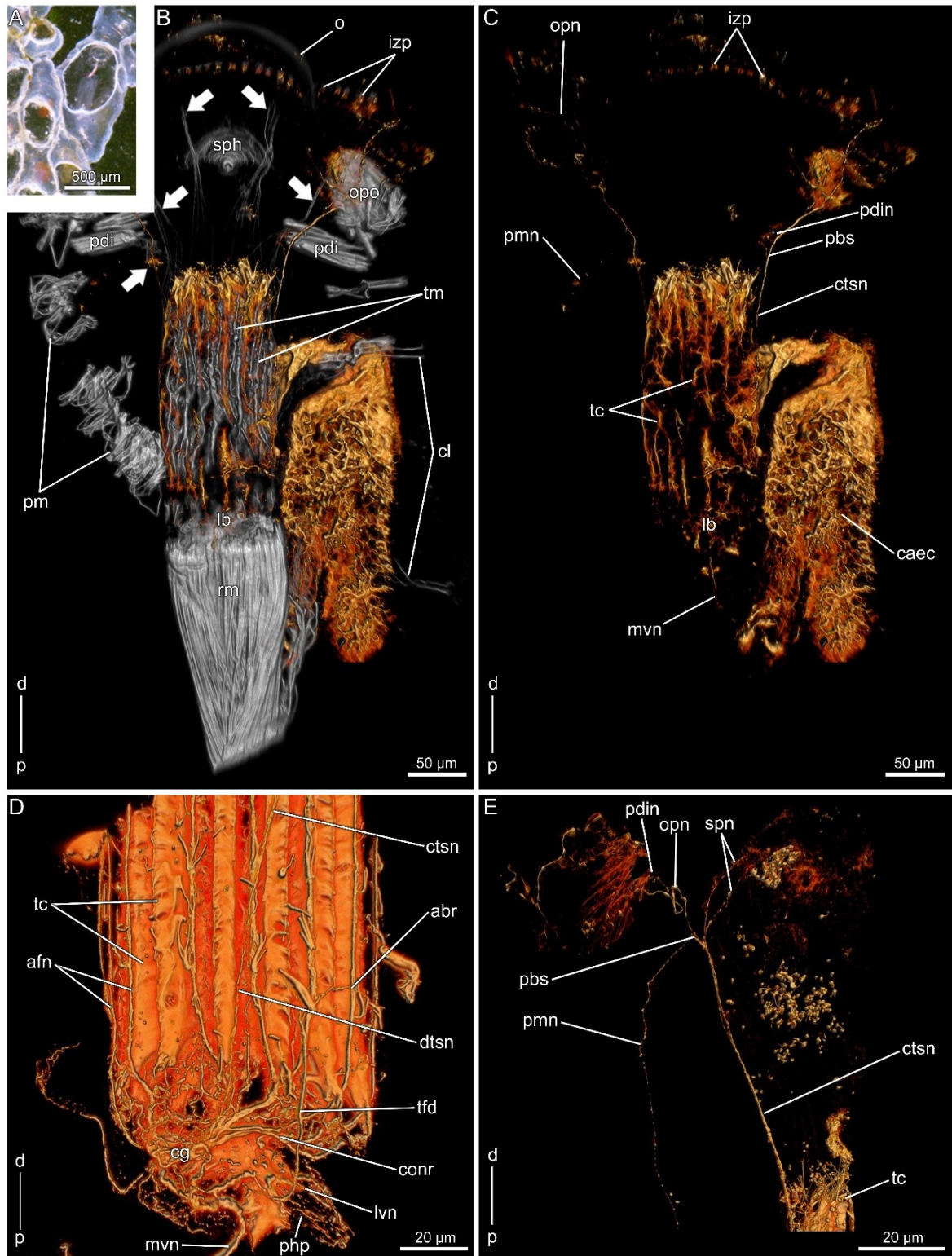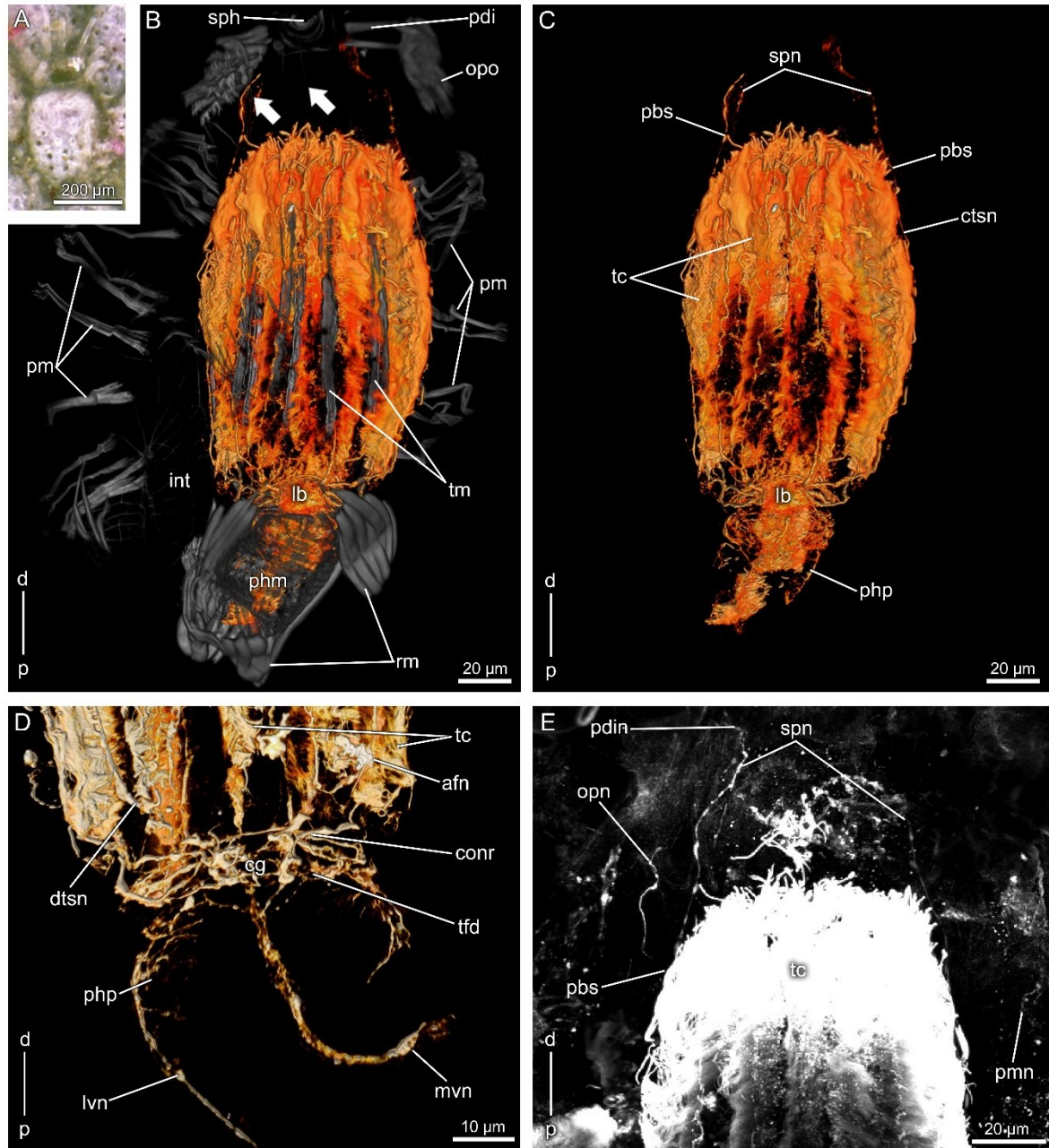
Figure 3: Acetylated α-tubulin-lir (orange) and f-actin (grey) structures in *Electra posidoniae*. **A** Overview of few zooids. **B** Overview of the animal from frontal, showing α-tubulin-lir and f-actin structures. **C** Overview of the animal from frontal, showing α-tubulin-lir structures. **D** Detail of the lophophoral base. **E** Detail of vestibular region.

Abbreviations: **abr** – annular branch of the trifid nerve, **afn** – abfrontal tentacle nerve, **caec** – caecum cilia, **cl** – caecum ligament, **cg** – cerebral ganglion, **conr** – circumoral nerve ring, **ctsn** – compound tentacle sheath nerve, **d** – distal, **izp** – interzooidal pores, **dtsn** – direct tentacle sheath nerve, **lb** – lophophoral base, **lvn** – laterovisceral nerve, **mvn** – mediovisceral nerve, **o** – operculum, **opn** – opercular nerve, **opo** – operculum occlusor muscle, **p** – proximal, **pbs** – parietal branching site, **pdi** – parietodiaphragmatic muscle, **pdin** – parietodiaphragmatic nerve, **php** – pharyngeal nerve plexus, **pm** – parietal muscle, **pmn** – parietal muscle nerve, **rm** – retractor muscle, **sph** – sphincter muscle, **spn** – sphincter nerve, **tc** – tentacle cilia, **tfd** – trifid nerve, **tm** – tentacle muscle bands, white arrows indicate the position of duplicature bands.
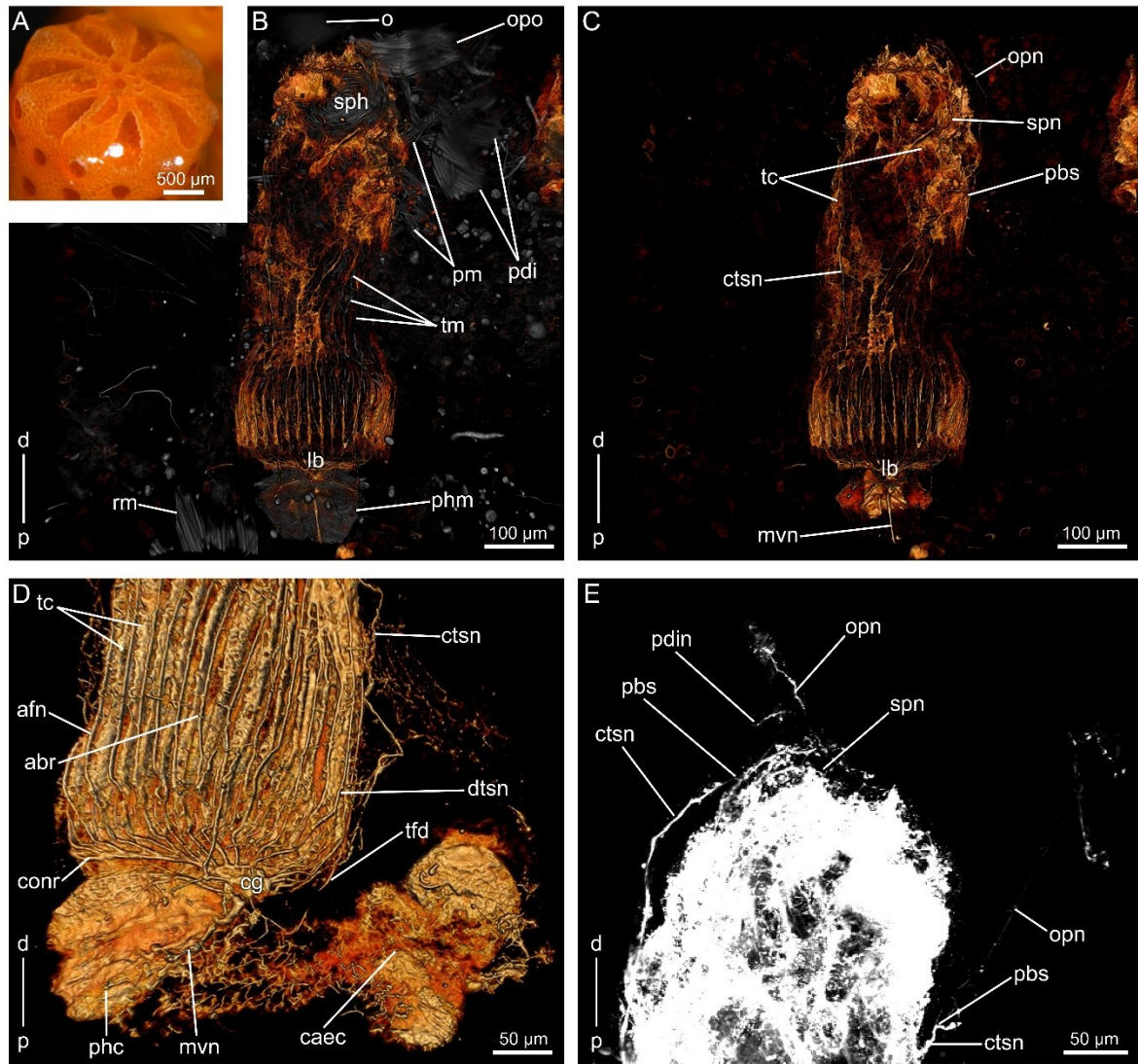
Figure 4: Acetylated α-tubulin-lir (orange) and f-actin (grey) structures in *Fenestrulina joannae*. **A** Overview of a zooid. **B** Overview of the animal from frontal, showing α-tubulin-lir and f-actin structures. **C** Overview of the animal from frontal, showing α-tubulin-lir structures. **D** Detail of the lophophoral base. **E** Detail of vestibular region.

Abbreviations: **afn** – abfrontal tentacle nerve, **cg** – cerebral ganglion, **conr** – circumoral nerve ring, **ctsn** – compound tentacle sheath nerve, **d** – distal, **dtsn** – direct tentacle sheath nerve, **int** – intestine, **lb** – lophophoral base, **lvn** – laterovisceral nerve, **mvn** – mediovisceral nerve, **opn** – opercular nerve, **opo** – operculum occlusor muscle, **p** – proximal, **pbs** – parietal branching site, **pdi** – parietodiaphragmatic muscle, **pdin** – parietodiaphragmatic nerve, **phm** – pharyngeal musculature, **php** – pharyngeal nerve plexus, **pm** – parietal muscle, **pmn** – parietal muscle nerve, **rm** – retractor muscle, **sph** – sphincter muscle, **spn** – sphincter nerve, **tc** – tentacle cilia, **tfd** – trifid nerve, **tm** – tentacle muscle bands.
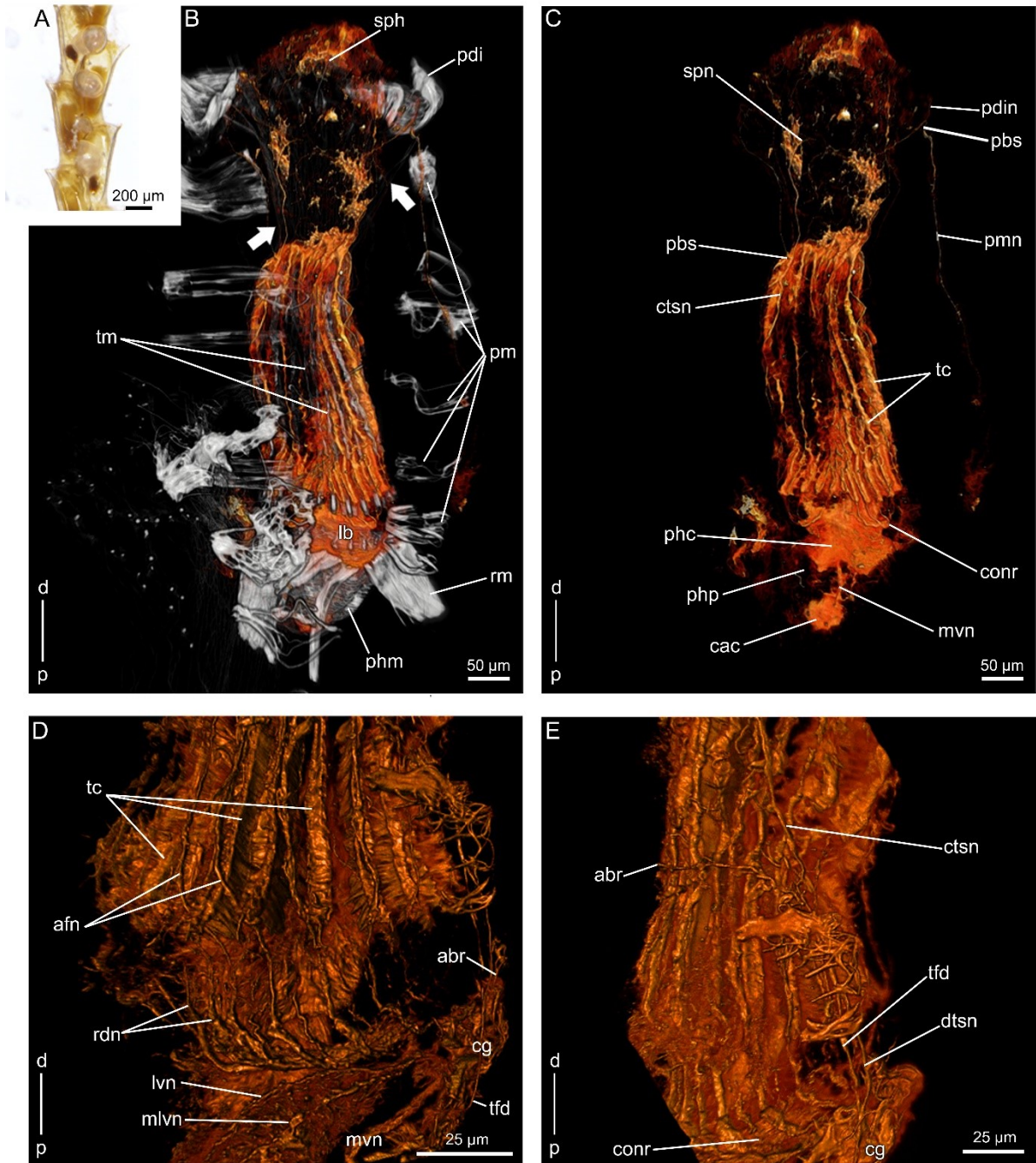
Figure 5: Acetylated α-tubulin-lir (orange) and f-actin (grey) structures in *Myriapora truncata*. **A** Overview of a few zooids. **B** Overview of the animal from basal, showing α-tubulin-lir and f-actin structures. **C** Overview of the animal from basal, showing α-tubulin-lir structures. **D** Detail of the lophophoral base. **E** Detail of vestibular region.

Abbreviations: **abr** – annular branch of trifid nerve, **afn** – abfrontal tentacle nerve, **caec** – caecum cilia, **cg** – cerebral ganglion, **conr** – circumoral nerve ring, **ctsn** – compound tentacle sheath nerve, **d** – distal, **dtsn** – direct tentacle sheath nerve, **lb** – lophophoral base, **mvn** – mediovisceral nerve, **o** – operculum, **opn** – opercular nerve, **opo** – operculum occlusor muscle, **p** – proximal, **pbs** – parietal branching site, **pdi** – parietodiaphragmatic muscle, **pdin** – parietodiaphragmatic nerve, **phm** – pharyngeal musculature, **pm** – parietal muscle, **pmn** – parietal muscle nerve, **rm** – retractor muscle, **sph** – sphincter muscle, **spn** – sphincter nerve, **tc** – tentacle cilia, **tfd** – trifid nerve, **tm** – tentacle muscle bands, white arrows indicate the position of duplicature bands.
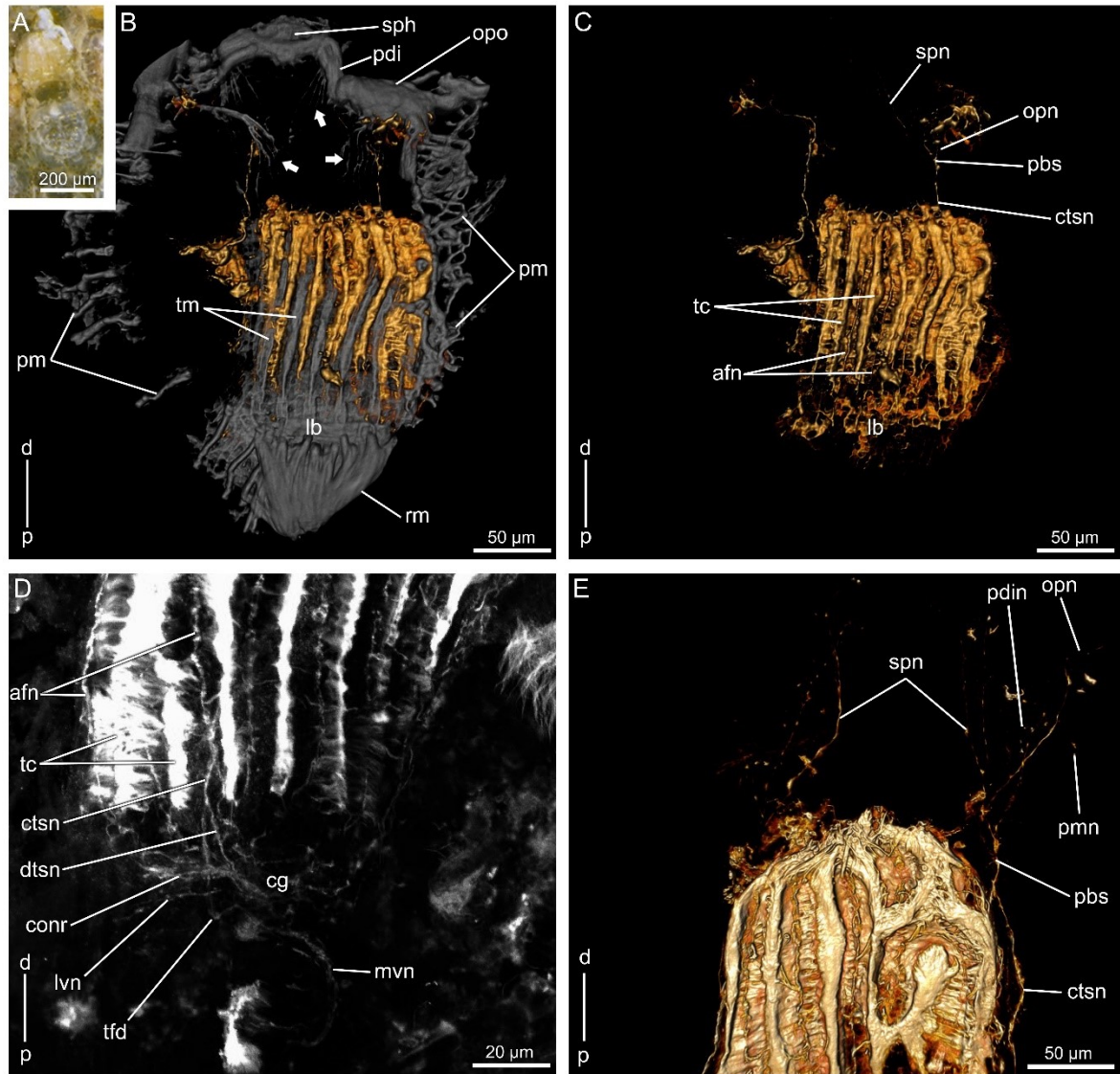
Figure 6: Acetylated α-tubulin-lir (orange) and f-actin (grey) structures in *Bugula neritina*. **A** Overview of few zooids. **B** Overview of the animal from frontal, showing α-tubulin-lir and f-actin structures. **C** Overview of the animal from frontal, showing α-tubulin-lir structures. **D** Detail of the lophophoral base in lateral view. **E** Detail of vestibular region in lateral view.

Abbreviations: **abr** – annular branch of trifid nerve, **afn** – abfrontal tentacle nerve, **cac** – cardia cilia, **cg** – cerebral ganglion, **conr** – circumoral nerve ring, **ctsn** – compound tentacle sheath nerve, **d** – distal, **dtsn** – direct tentacle sheath nerve, **lb** – lophophoral base, **lvn** – laterovisceral nerve, **mlvn** – mediolaterovisceral nerve, **mvn** – mediovisceral nerve, **p** – proximal, **pbs** – parietal branching site, **pdi** – parietodiaphragmatic muscle, **pdin** – parietodiaphragmatic nerve, **phm** – pharyngeal musculature, **php** – pharyngeal nerve plexus, **pm** – parietal muscle, **pmn** – parietal muscle nerve, **rdn** – radial nerve, **rm** – retractor muscle, **sph** – sphincter muscle, **spn** – sphincter nerve, **tc** – tentacle cilia, **tfd** – trifid nerve, **tm** – tentacle muscle bands, white arrows indicate the position of duplicature bands.
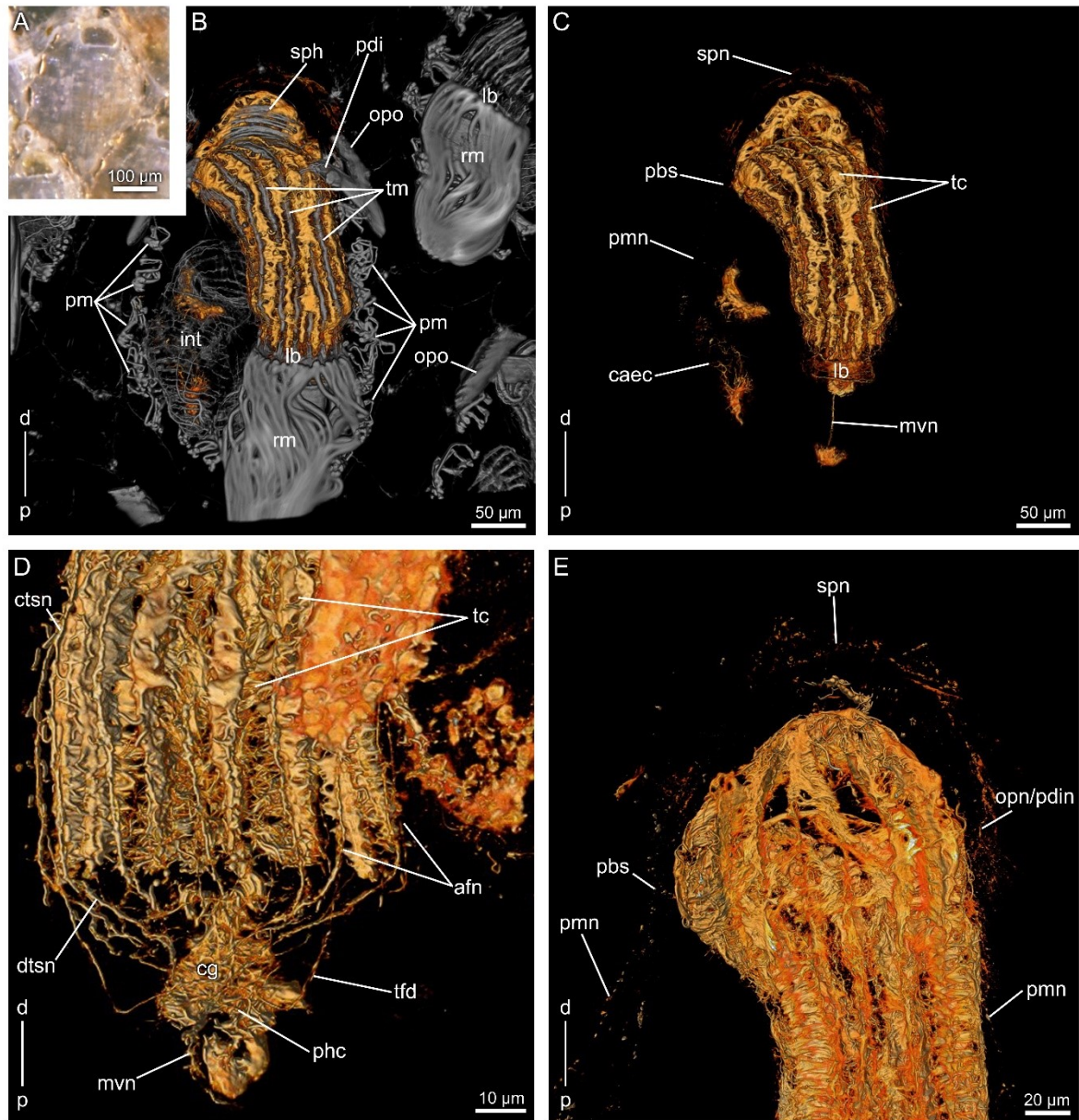
Figure 7: Acetylated α-tubulin-lir (orange) and f-actin (grey) structures in *Collarina balzaci*. **A** Overview of a zooid. **B** Overview of the animal from frontal, showing α-tubulin-lir and f-actin structures. **C** Overview of the animal from frontal, showing α-tubulin-lir structures. **D** Detail of the lophophoral base. **E** Detail of vestibular region.

Abbreviations: **afn** – abfrontal tentacle nerve, **cg** – cerebral ganglion, **conr** – circumoral nerve ring, **ctsn** – compound tentacle sheath nerve, **d** – distal, **dtsn** – direct tentacle sheath nerve, **lb** – lophophoral base, **lvn** – laterovisceral nerve, **mvn** – medioviseral nerve, **opn** – opercular nerve, **opo** – operculum occlusor muscle, **p** – proximal, **pbs** – parietal branching site, **pdi** – parietodiaphragmatic muscle, **pdin** – parietodiaphragmatic nerve, **pm** – parietal muscle, **pmn** – parietal muscle nerve, **rm** – retractor muscle, **sph** – sphincter muscle, **spn** – sphincter nerve, **tc** – tentacle cilia, **tfd** – trifid nerve, **tm** – tentacle muscle bands, white arrows indicate the position of duplicature bands.

Figure 8: Acetylated a- tubulin-lir (orange) and f-actin (grey) structures in *Chorizopora brongniartii*. **A** Overview of a zooid. **B** Overview of the animal from frontal, showing α-tubulin-lir and f-actin structures. **C** Overview of the animal from frontal, showing α-tubulin-lir structures. **D** Detail of the lophophoral base. **E** Detail of vestibular region.

Abbreviations: **afn** – abfrontal tentacle nerve, **caec** – caecum cilia, **cg** – cerebral ganglion, **ctsn** – compound tentacle sheath nerve, **d** – distal, **dtsn** – direct tentacle sheath nerve, **int** – intestine, **lb** – lophophoral base, **mvn** – mediovisceral nerve, **opn** – opercular nerve, **opo** – operculum occlusor muscle, **p** – proximal, **pbs** – parietal branching site, **pdi** – parietodiaphragmatic muscle, **pdin** – parietodiaphragmatic nerve, **phc** – pharyngeal cilia, **pm** – parietal muscle, **pmn** – parietal muscle nerve, **rm** – retractor muscle, **sph** – sphincter muscle, **spn** – sphincter nerve, **tc** – tentacle cilia, **tfd** – trifid nerve, **tm** – tentacle muscle bands.
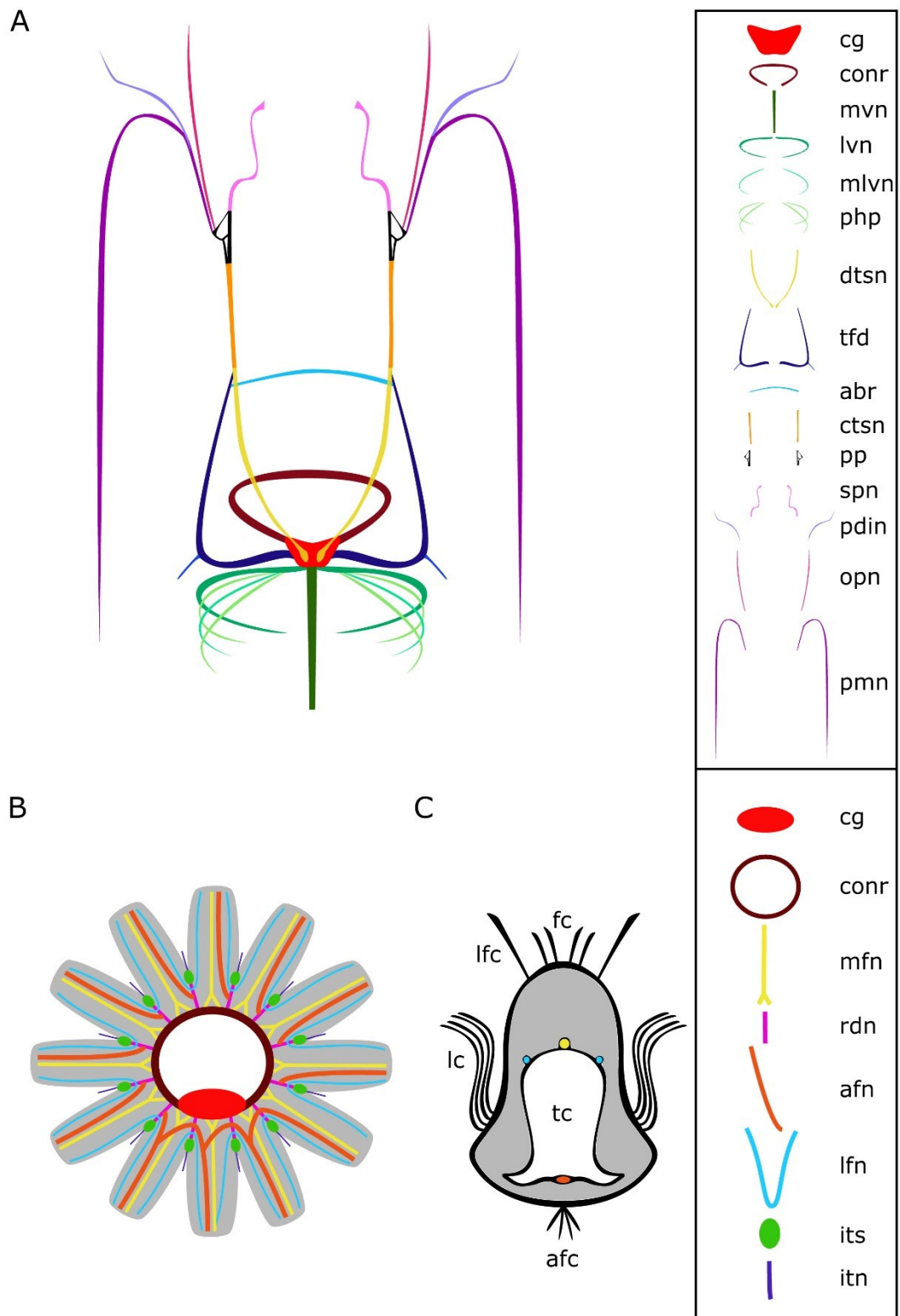
Figure 9: Ground pattern of the autozooidal innervation in cheilostomes. **A** Basal view of the autozooidal innervation pattern without lophophore. **B** Oral view on the innervation pattern of the lophophore in protruded condition **C** Cross section of a tentacle modified from Schwaha (in press).

Abbreviations: **abr** – annular branch of trifid nerve, **afc** – abfrontal cilia, **afn** – abfrontal tentacle nerve, **cg** – cerebral ganglion, **conr** – circumoral nerve ring, **ctsn** – compound tentacle sheath nerve, **dtsn** – direct tentacle sheath nerve, **fc** – frontal cilia, **itn** – intertentacular neurite, **its** – intertentacular site, **lc** – lateral cilia, **lfc** – laterofrontal cilia, **lfn** – laterofrontal tentacle nerve, **lvn** – laterovisceral nerve, **mfn** – mediofrontal tentacle nerve, **mlvn** – mediolaterovisceral nerve, **mvn** – mediovisceral nerve, **pbs** – parietal branching site, **pdin** – parietodiaphragmatic nerve, **php** – pharyngeal nerve plexus, **pmn** – parietal muscle nerve, **opn** – opercular nerve, **rdn** – radial nerve, **spn** – sphincter nerve, **tc** – tentacle coeloma, **tfd** – trifid nerve.
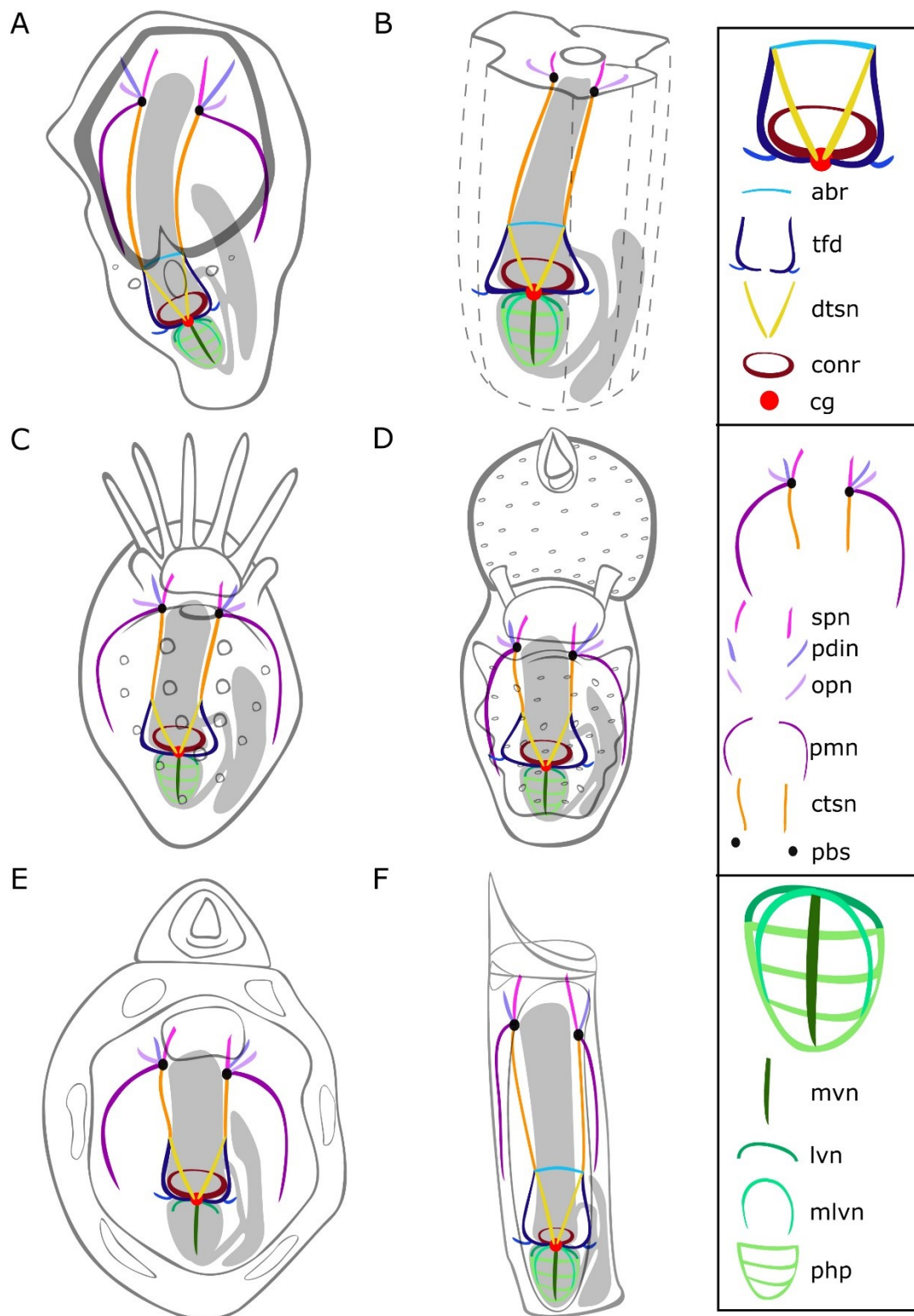
Figure 10: Innervation schemes based on data from this study. **A** *Electra posidoniae*. **B** *Myriapora truncata*. **C** *Fenestrulina joannae*. **D** *Collarina balzaci*. **E** *Chorizopora brongniartii*. **F** *Bugula neritina*.

Abbreviations: **abr** – annular branch of trifid nerve, **cg** – cerebral ganglion, **conr** – circumoral nerve ring, **ctsn** – compound tentacle sheath nerve, **dtsn** – direct tentacle sheath nerve, **lvn** – laterovisceral nerve, **mlvn** – mediolaterovisceral nerve, **mvn** – medioviceral nerve, **pbs** – parietal branching site, **pdin** – parietodiaphragmatic nerve, **php** – pharyngeal nerve plexus, **pmn** – parietal muscle nerve, **opn** – opercular nerve, **spn** – sphincter nerve, **tfd** – trifid nerve.
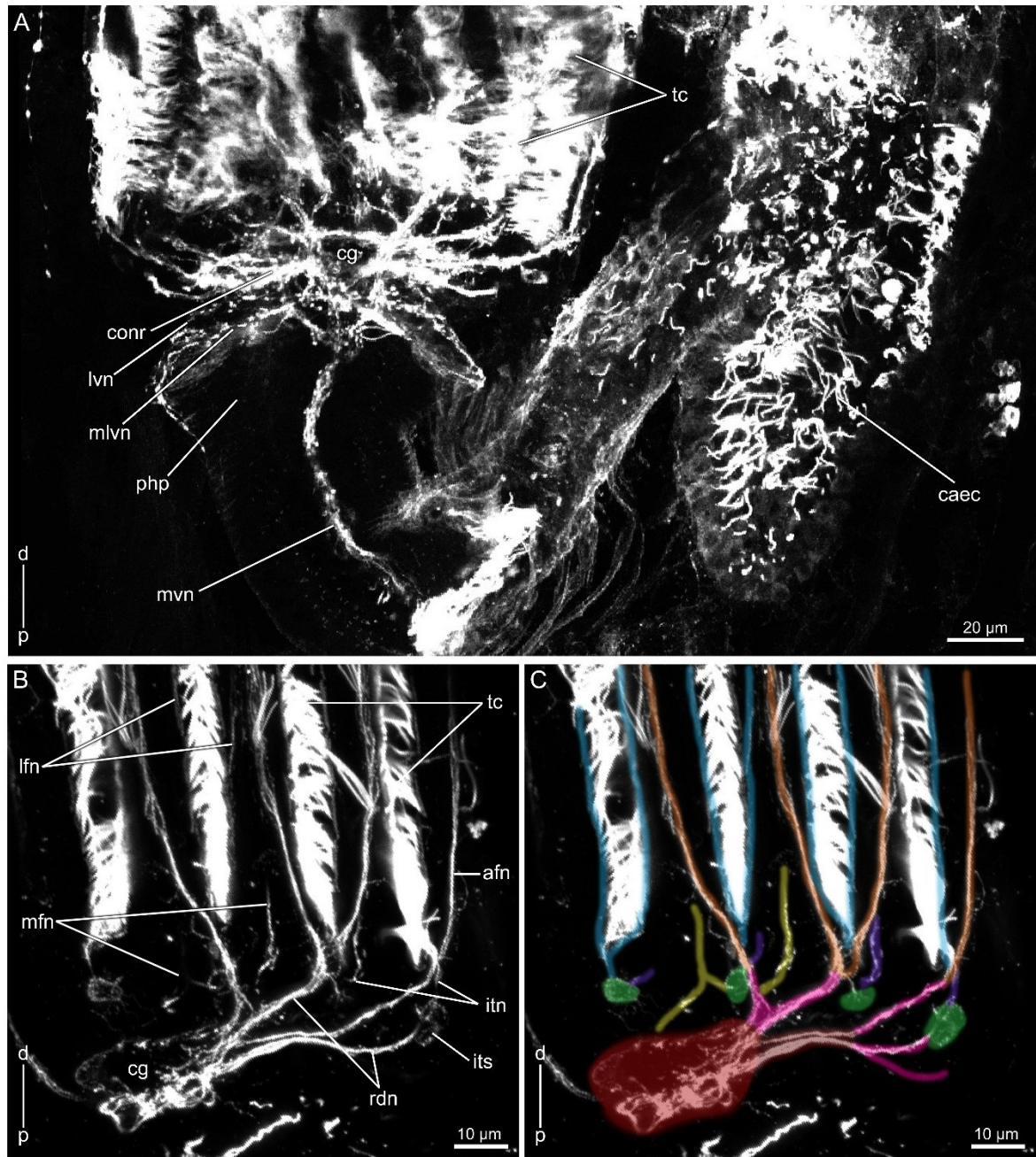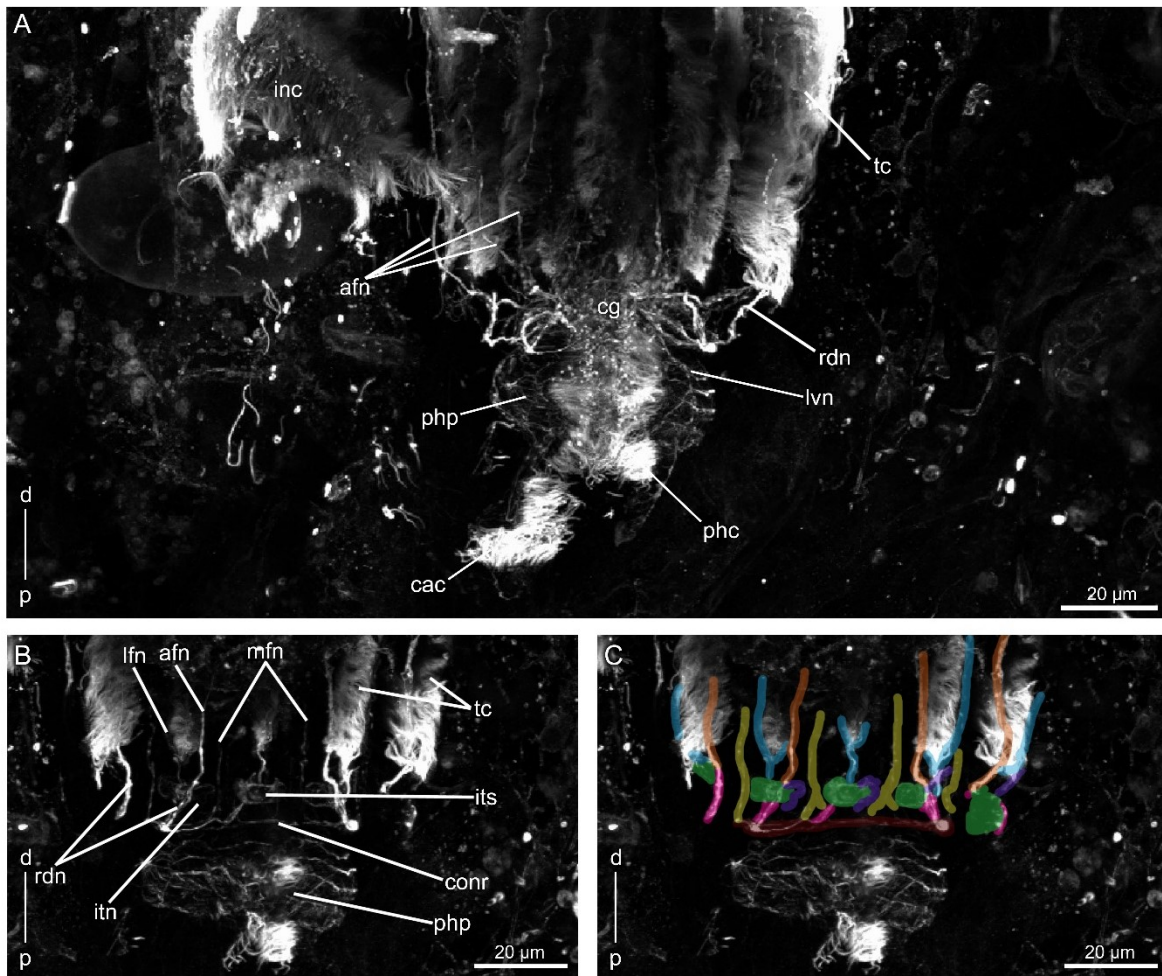
Figure 11: Acetylated α-tubulin-lir structures in the lophophore of *Electra posidoniae.* **A** Detail of the lophophoral base and of the digestive tract. **B** Detail of tentacular innervation at the lophophoral base. **C** Detail of tentacular innervation at the lophophoral base labelled with a color code. Abbreviations and color code: **afn** – abfrontal tentacle nerve (orange), **caec** – caecal cilia, **cg** – cerebral ganglion (red), **conr** – circumoral nerve ring (brown), **d** – distal, **itn** – intertentacular neurite (purple), **its** – intertentacular site (green), **lfn** – laterofrontal tentacle nerve (blue), **lvn** – laterovisceral nerve, **mfn** – mediofrontal tentacle nerve (yellow), **mlvn** –

mediolateroisceral nerve, **mvn** – medioisceral nerve, **p** – proximal, **php** – pharyngeal nerve plexus, **rdn** – radial nerve (pink), **tc** – tentacle cilia.

Figure 12: Acetylated α-tubulin-lir structures in the lophophore of *Fenestrulina joannae.* **A** Detail of the lophophoral base and the visceral tract. **B** Detail of tentacular innervation at the lophophoral base. **C** Detail of tentacular innervation at the lophophoral base labelled with a color code. Abbreviations and color code: **afn** – abfrontal tentacle nerve (orange), **cac** – cardia cilia, **cg** – cerebral ganglion (red), **conr** – circumoral nerve ring (brown), **d** - distal, **itn** – intertentacular neurite (purple), **inc** – intestinal cilia, **its** – intertentacular site (green), **lfn** – laterofrontal tentacle nerve (blue), **lvn** – laterovisceral nerve, **mfn** – mediofrontal tentacle nerve (yellow), **p** – proximal, **phc** – pharyngeal cilia, **php** – pharyngeal nerve plexus, **rdn** – radial nerve (pink), **tc** – tentacle cilia.
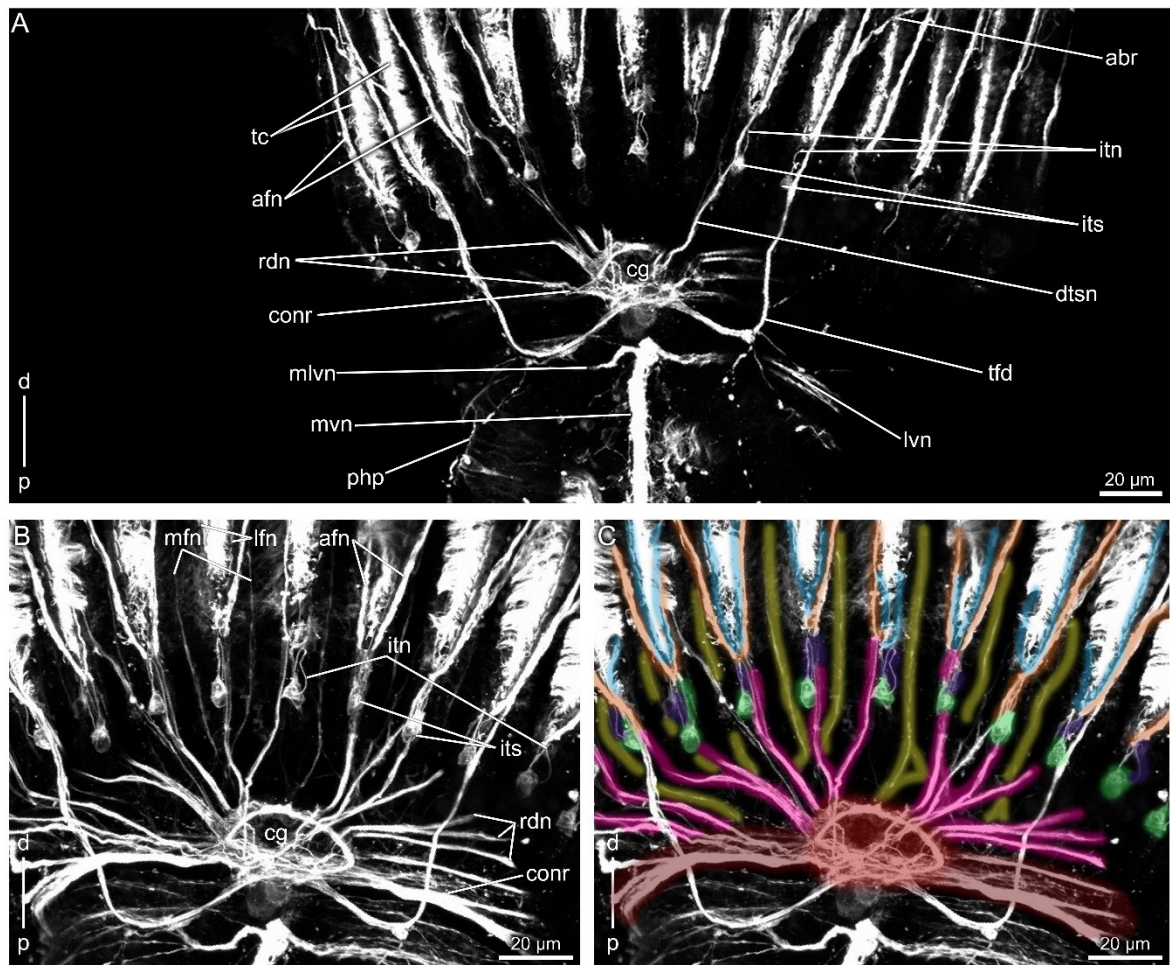
Figure 13: Acetylated α-tubulin-lir structures in the lophophore of *Myriapora truncata*. **A** Detail of the lophophoral base. **B** Detail of tentacular innervation at the lophophoral base. **C** Detail of tentacular innervation at the lophophoral base labelled with a color code. Abbreviations and color code: **abr** – annular branch of trifid nerve, **afn** – abfrontal tentacle nerve (orange), **cg** – cerebral ganglion (red), **conr** – circumoral nerve ring (brown), **d** – distal, **dtsn** – direct tentacle sheath nerve, **itn** – intertentacular neurite (purple), **its** – intertentacular site (green), **lfn** – laterofrontal tentacle nerve (blue), **lvn** – laterovisceral nerve, **mfn** – mediofrontal tentacle nerve (yellow), **mlvn** – mediolaterovisceral nerve, **mvn** – mediovisceral nerve, **p** – proximal, **php** – pharyngeal nerve plexus, **rdn** – radial nerve (pink), **tc** – tentacle cilia, **tfd** – trifid nerve.
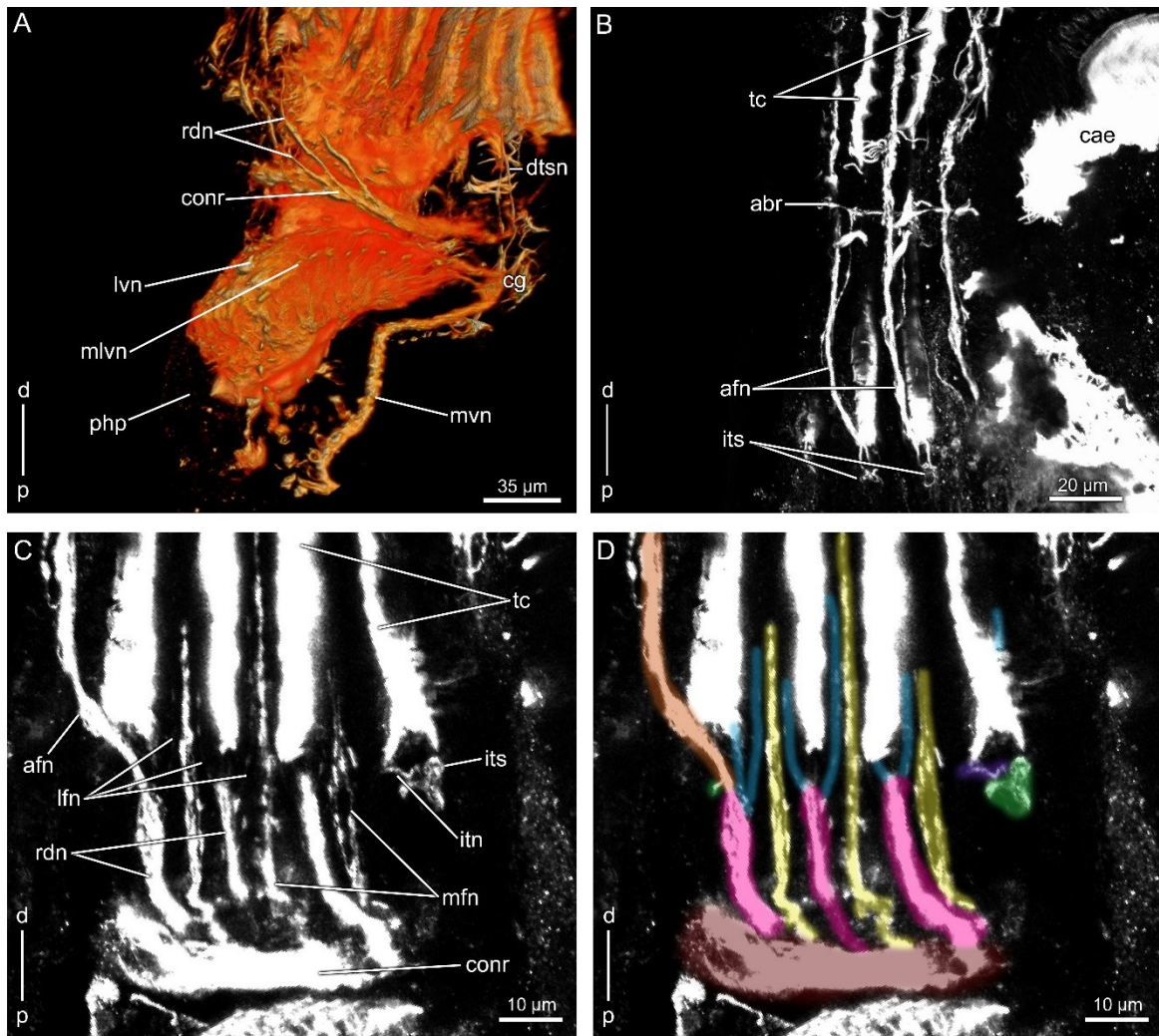
Figure 14: Acetylated α-tubulin-lir structures in the lophophore of *Bugula neritina.* **A** Detail of the lophophoral base. **B** Detail of the annular branch of trifid nerve. **C** Detail of tentacular innervation at the lophophoral base. **D** Detail of tentacular innervation at the lophophoral base labelled with a color code. Abbreviations and color code: **abr** – annular branch of trifid nerve, **afn** – abfrontal tentacle nerve (orange), **cae** – caecum, **cg** – cerebral ganglion (red), **conr** – circumoral nerve ring (brown), **d** – distal, **dtsn** – direct tentacle sheath nerve, **itn** – intertentacular neurite (purple), **its** – intertentacular site (green), **lfn** – laterofrontal tentacle nerve (blue), **lvn** – laterovisceral nerve, **mfn** – mediofrontal tentacle nerve (yellow), **mlvn** – mediolaterovisceral nerve, **mvn** – medioviscéral nerve, **p** – proximal, **php** – pharyngeal nerve plexus, **rdn** – radial nerve (pink), **tc** – tentacle cilia.
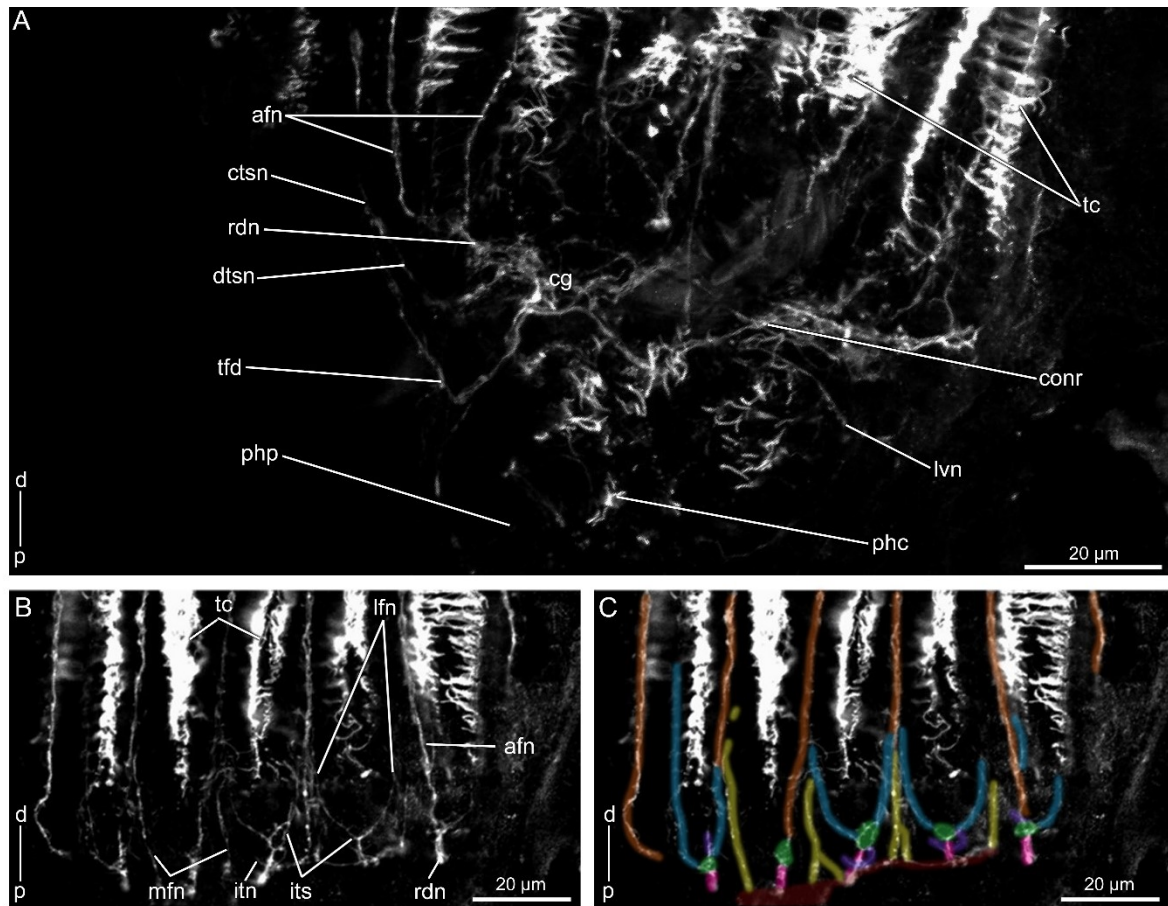
Figure 15: Acetylated α-tubulin-lir structures in the lophophore of *Collarina balzaci*. **A** Detail of the lophophoral base. **B** Detail of tentacular innervation at the lophophoral base. **C** Detail of tentacular innervation at the lophophoral base labelled with a color code. Abbreviations and color code: **afn** – abfrontal tentacle nerve (orange), **cg** – cerebral ganglion (red), **conr** – circumoral nerve ring (brown), **ctsn** – compound tentacle sheath nerve, **d** – distal, **dtsn** – direct tentacle sheath nerve, **itn** – intertentacular neurite (purple), **its** – intertentacular site (green), **lfn** – laterofrontal tentacle nerve (blue), **lvn** – laterovisceral nerve, **mfn** – mediofrontal tentacle nerve (yellow), **p** – proximal, **phc** – pharyngeal cilia, **php** – pharyngeal nerve plexus, **rdn** – radial nerve (pink), **tc** – tentacle cilia, **tfd** – trifid nerve.
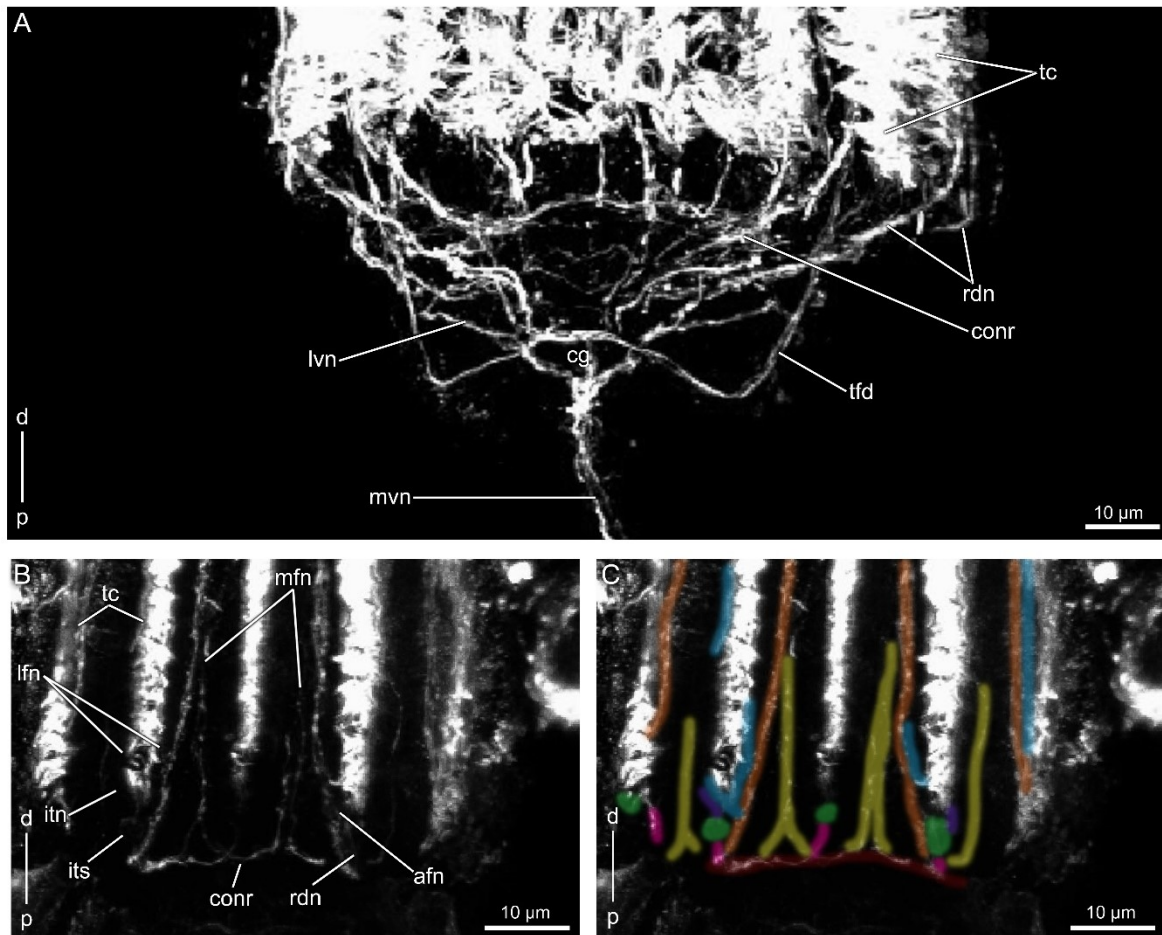
Figure 16: Acetylated α-tubulin-lir structures in the lophophore of *Chorizopora brongniartii.* **A** Detail of the lophophoral base. **B** Detail of tentacular innervation at the lophophoral base. **C** Detail of tentacular innervation at the lophophoral base labelled with a color code. Abbreviations and color code: **afn** – abfrontal tentacle nerve (orange), **cg** – cerebral ganglion (red), **conr** – circumoral nerve ring (brown), **d** – distal, **itn** – intertentacular neurite (purple), **its** – intertentacular site (green), **lfn** – laterofrontal tentacle nerve (blue), **lvn** – laterovisceral nerve, **mfn** – mediofrontal tentacle nerve (yellow), **mvn** – meddiovisceral nerve, **p** – proximal, **rdn** – radial nerve (pink), **tc** – tentacle cilia, **tfd** – trifid nerve.
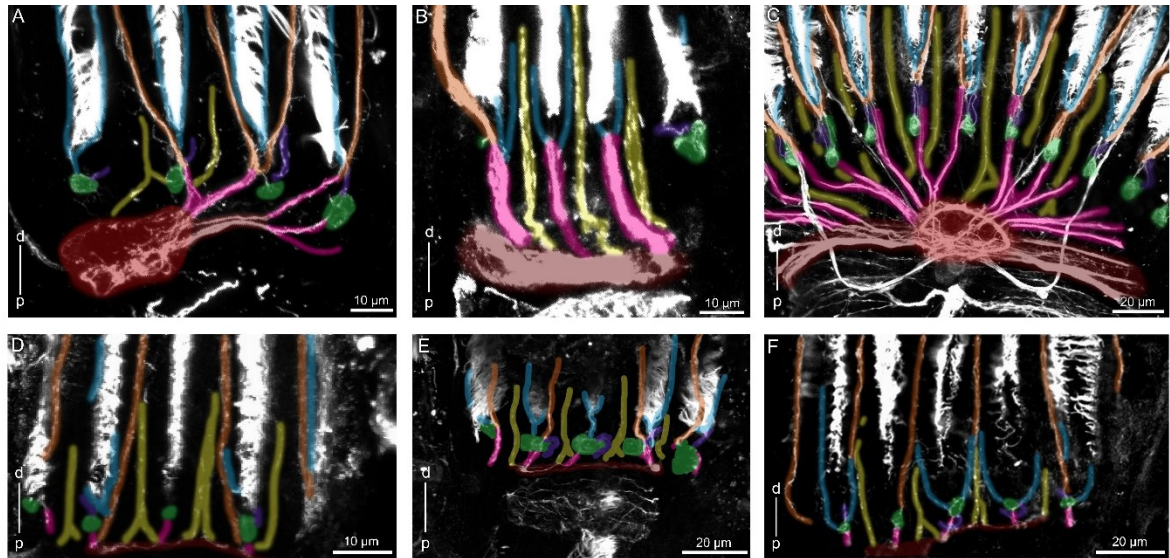
Figure 17: Details of the acetylated a α-tubulin-lir structures on the lophophoral base of six cheilostome species. **A** *Electra posidoniae*. **B** *Bugula neritina*. **C** *Myriapora truncata*. **D** *Chorizopora brongniartii*. **E** *Fenestrulina joannae*. **F** *Collarina balzaci*. Abbreviations and color code: abfrontal tentacle nerve (orange), cerebral ganglion (red), circumoral nerve ring (brown), **d** – distal, intertentacular neurite (purple), intertentacular site (green), laterofrontal tentacle nerve (blue), mediofrontal tentacle nerve (yellow), **p** – proximal, radial nerve (pink).
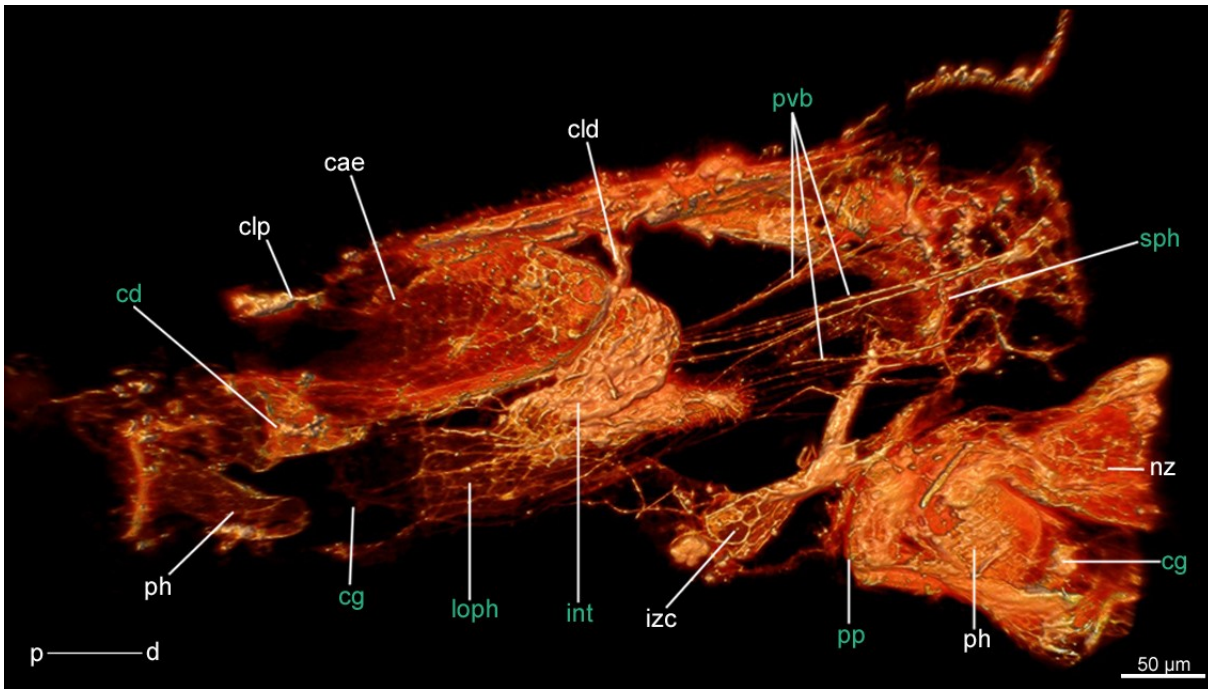
Figure 18: Neuronal tracing with DiI in *Electra posidoniae*. Abbreviations and color code: **cae** – caecum, **cd** – cardia, **cg** – cerebral ganglion, **cld** – distal caecum ligament, **clp** – proximal caecum ligament, **d** – distal, int – intestine, **izc** – interzooidal connection, **loph** – lophophore, **nz** – neighboring zooid, **p** – proximal, **ph** – pharynx, **pp** – pharyngeal plexus, **pvb** – duplicature bands, **sph** – sphincter. Acetylated α-tubulin-lir structures with green labels, remaining tissues with white labels.